Simulation of Air Flow Past the Opposed and Parallel Inclined Flat Plates in a Rectangular Duct

Satapan Phapatarinan

A Report Submitted in Partial Fulfillment of the Requirements
for the Degree of Bachelor of Engineering (Petrochemical Engineering)
Department of Chemical Engineering, Faculty of Engineering,
King Mongkut's Institute of Technology Ladkrabang
Academic Year 2016

การจำลองการไหลของอากาศผ่านแผ่นแบนเรียบที่เอียงขนานกันและที่เอียงทำมุมกันในท่อรูปสี่เหลี่ยมมุมฉาก

ศาตปัญญ์ ปภาธารินันท์

ปริญญานิพนธ์นี้เป็นส่วนหนึ่งของการศึกษาตามหลักสูตร
วิศวกรรมศาสตรบัณฑิต สาขาวิชาวิศวกรรมปิโตรเคมี
ภาควิชาวิศวกรรมเคมี คณะวิศวกรรมศาสตร์
สถาบันเทคโนโลยีพระจอมเกล้าเจ้าคุณทหารลาดกระบัง
ปีการศึกษา 2559

Title	Simulation of Air Flow Past the Opposed and Parallel Inclined Flat Plates in a Rectangular Duct
By	Mr. Satapan Phapatarinan
Field of Study	Petrochemical Engineering
Advisor	Asst. Prof. Dr. Santi Wattananusorn

Accepted by the Faculty of Engineering, King Mongkut's Institute of Technology Ladkrabang in Partial Fulfillment of the Requirements for the Degree of Bachelor of Engineering (Petrochemical Engineering).

Thesis Committee

W. Santi

(Asst. Prof. Dr. Santi Wattananusorn) Chairman

Walairat Chandra-ambhorn

(Asst. Prof. Dr. Walairat Chandra-ambhorn) Committee

(Dr. Amata Anantpinijwatna) Committee

Title	Simulation of Air Flow Past the Opposed and Parallel Inclined Flat Plates in a Rectangular Duct
By	Mr. Satapan Phapatarinan
Advisor	Asst. Prof. Dr. Santi Wattananusorn
Field of Study	Petrochemical Engineering
Affiliation	Faculty of Engineering, King Mongkut's Institute of Technology Ladkrabang

Abstract

In air-handling systems, dampers are used to ensure the proper operation of the various air systems. When the damper is presented in the duct, there is an effect of installation on the flowrate measurement in downstream. If a flow measuring devices are located within this region, the accuracy of the flow measurement is reduced. The objectives of this research are to study the phenomena of laminar and turbulent flows through the inclined flat plates in a horizontal rectangular duct and two different types of damper, including parallel-blades and opposed-blades, by using computational fluid dynamics (CFD) technique. In addition, blades alignment was also investigated. The ANSYS FLUENT 14.5 finite volume CFD code was adopted to solve steady state three-dimensional flow inside the duct. The Reynolds averaged equations with standard k-ε turbulence model were used to simulate the mean flow properties and turbulence. The simulated results revealed that the laminar flow exhibited the longer entrance length as compared to the turbulent flow. The entrance lengths of opposed-blades were shorter than the parallel-blades. Further, the entrance length was also affected by blades alignment.

Keywords: simulation, computational fluid dynamics, air flow, flat plates, damper.

เรื่อง การจำลองการไหลของอากาศผ่านแผ่นแบนเรียบที่เอียงขนานกันและที่เอียงทำมุมกันในท่อรูปสี่เหลี่ยมมุมฉาก
โดย นายศาตปัญญ์ ปภาธารินันท์
อาจารย์ที่ปรึกษา ผศ.ดร.สันติ วัฒนานุสรณ์
สาขาวิชา วิศวกรรมปิโตรเคมี
สังกัด คณะวิศวกรรมศาสตร์ สถาบันเทคโนโลยีพระจอมเกล้าเจ้าคุณทหารลาดกระบัง

บทคัดย่อ

ในระบบจัดการอากาศ แดมเปอร์ถูกใช้สำหรับยืนยันการทำงานที่ถูกต้องของระบบ เมื่อแดมเปอร์ชนิดต่าง ๆได้ถูกติดตั้งในท่อจะเกิดอิทธิพลของการติดตั้งต่อการวัดอัตราการไหลที่ปลายทาง หากอุปกรณ์วัดอัตราการไหลถูกติดตั้งภายในระยะนี้ จะทำให้ความแม่นยำในการวัดลดน้อยลง จุดประสงค์ของงานวิจัยนี้คือการศึกษาปรากฏการณ์ของการไหลแบบราบเรียบและการไหลแบบปั่นป่วนที่ไหลผ่านแผ่นแบนเรียบเอียงในท่อรูปสี่เหลี่ยมมุมฉากแนวนอน ซึ่งใช้แดมเปอร์ 2 ชนิดที่ต่างกัน คือ เอียงขนานกันและเอียงทำมุมกัน โดยใช้เทคนิคพลศาสตร์ของไหลเชิงคำนวณ ทั้งนี้ยังมีการตรวจสอบการจัดเรียงของแผ่นเรียบอีกด้วย โปรแกรม ANSYS FLUENT 14.5 ถูกนำมาใช้เพื่อหาคำตอบสำหรับการไหลในท่อที่สถานะคงตัวในสามมิติภายใต้หลักการของไฟไนต์โวลุ่ม สมการเรย์โนลด์ในรูปค่าเฉลี่ยเสริมด้วยแบบจำลองการไหลแบบปั่นป่วน standard k-ε ถูกนำมาใช้เพื่อจำลองหาสมบัติต่าง ๆของการไหลและความปั่นป่วน ซึ่งผลการจำลองได้แสดงให้เห็นว่าการไหลแบบราบเรียบมีระยะทางซึ่งใช้ในการปรับตัวเข้าสู่สภาวะการไหลคงรูปที่มากกว่าการไหลแบบปั่นป่วน และแดมเปอร์ชนิดเอียงทำมุมกันยังให้ระยะข้างต้นน้อยกว่าชนิดเอียงขนานกัน นอกจากนี้ระยะดังกล่าวยังได้รับผลกระทบจากการจัดเรียงของแผ่นเรียบอีกด้วย

คำสำคัญ: การจำลอง, พลศาสตร์ของไหลเชิงคำนวณ, การไหลของอากาศ, แผ่นแบนเรียบ, แดมเปอร์

Acknowledgements

Foremost, I would like to acknowledge my thesis advisor, Asst. Prof. Dr. Santi Wattananusorn for educate a knowledge about fluid dynamics and also the theories used in solving problems other than fluid dynamics to complete this thesis successfully completed.

I am very thankful to my friends for their helpful and encouraging guidance throughout the course of this work. In addition, I am also thankful to Department of Chemical Engineering, King Mongkut's Institute of Technology Ladkrabang for opportunities and undergraduate life.

Furthermore, I would like to thank all members of Computational Fluid Dynamics Laboratory for their help, suggestion and warm collaborations.

Finally, I would like to express my cordial and deep thanks to my family for providing the necessary atmosphere of understanding and all supporting for me.

Satapan Phapatarinan

Contents

Contents (continued)

Contents (continued)

List of Tables

List of Figures

List of Figures (continued)

List of Figures (continued)

List of Figures (continued)

List of Abbreviations

ALPHABETICAL SYMBOLS

A	Section of body
C	Circumference
C_D	Drag coefficient
C_L	Lift coefficient
C_μ	Empirical constant
C_1, C_2	Coefficient in approximated turbulent transport equation
D	Duct diameter
D_h	Hydraulic diameter
F_D	Drag force
F_F	Friction drag
F_L	Lift force
G_b	The generation of turbulent due to buoyancy
G_k	The production of turbulent due to buoyancy
g	Gravitational force
k	Turbulent kinetic energy
L_e	Entrance length
p	Pressure
$\bar{p}$	Mean value of pressure

List of Abbreviations (continued)

p'	Fluctuating component of pressure
Re	Reynolds number in pipe flow
S_k	Turbulent kinetic energy source term
S_{Mx}, S_{My}, S_{Mz}	Momentum source term in x, y, z directions
S_ε	Dissipation rate of turbulent kinetic energy source term
u, v, w	Velocity components in x, y, z directions
V	Fluid mean velocity
x, y, z	Rectangular coordinates

GREEK SYMBOLS

β	Thermal expansion coefficient
ε	Dissipation rate of turbulent kinetic energy
μ	Viscosity
μ_t	Turbulent viscosity
μ_{eff}	Effective viscosity
ρ	Fluid density
$\tau_{xx}, \tau_{yy}, \tau_{zz}$	Normal stresses on y-z, x-z, x-y planes
$\tau_{xy}, \tau_{xz}, \tau_{yz}$	Shear stresses on y-z, x-z, x-y planes

CHAPTER I

INTRODUCTION

1.1 Background and motivation

A damper is a valve or plate that stops or regulates the air flow inside a duct or other air handling equipment. Damper consists of one or more vanes, doors, hinges or pivot blades, which can be rotated to various position for controlling the air flow or other air handling equipment (see Figure 1.1). The operation of damper can be manual or automatic. Manual dampers are turned by handle on the outside of a duct. Automatic dampers are used to regulate airflow constantly and are operated by electric or pneumatic motors (see Figure 1.2) [1].

The single blade damper is generally restricted to small sizes since it does not provide accurate control. When fitted in circular ductwork it is referred to as a butterfly damper. A multi-blade or louvre damper has two or more blades linked together. Two basic styles of multi-blade damper construction are (see Figure 1.3).

- The parallel-blade damper: it has adjacent blades linked to rotate in the same direction when operated.
- The opposed-blade damper: it has adjacent blades linked to rotate in opposite directions when operated.

When any type of damper is presented in the duct, there is an effect on the measuring of the flowrate in downstream direction, is so called installation effect. If a flow measuring devices are located within a range of this effect, the accuracy of the flow measurement will be reduced.

To avoid the installation effect, the measuring devices should be installed in the fully developed flow region. Nevertheless, the region varied with upstream flow conditions (downstream flow of the damper) mostly depending on flowrate, configuration of the damper and duct, and air properties such as viscosity.

In this project, the phenomena of the fluid flow past the axisymmetric body with various types of damper (installation effect) and blades alignment are numerically studied. These simulations help the users to determine the region where the installation effect is absence, which is commonly called the region of fully developed flow.

1.2 Objective

To study the phenomena of fluid flow past the opposed and parallel inclined flat plates in a rectangular duct for determine the regions of fully developed flow in various conditions using the computational fluid dynamics (CFD) technique.

1.3 Scopes of research

1.3.1 Validation of simulation model; Comparison between simulation results and experimental results

1.3.2 Employ CFD technique using the ANSYS FLUENT 14.5 to study the phenomena of fluid flow past the inclined flat plates in a rectangular duct. The following parameters are investigated for their effects on the entrance length.

- Effect of flow characteristic, including laminar flow and turbulent flow
- Effect of damper's type, including opposed blade and parallel blade
- Effect of blade alignment

1.4 Educational processes

1.4.1 The damper geometry in a square duct as reported by Wattananusorn [2] is conducted to study the grid independency and to validate the present model.

1.4.2 The models are used to study the influence of flow characteristic, type of damper and blade alignment on the entrance length when fluid flow in the rectangular duct.

1.5 Expected benefit

Obtain the knowledge of measuring device installation in the rectangular duct for various engineering applications.

Figure 1.1 Damper

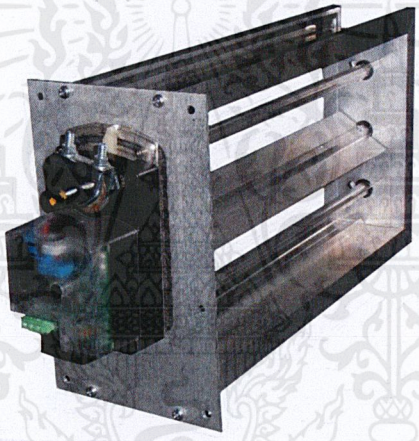

Figure 1.2 Automatic control damper

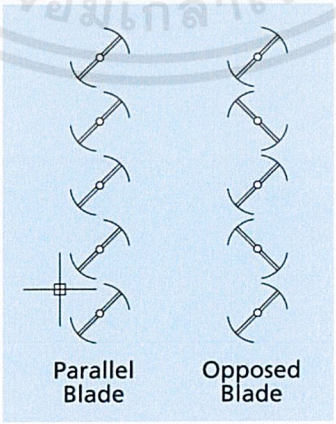

Figure 1.3 Damper blade arrangement

CHAPTER II

THEORY AND LITERATURE REVIEW

2.1 Computational fluid dynamics (CFD)

Computational fluid dynamics or CFD is a branch of fluid mechanics that uses numerical technique and algorithm to solve and analyze various flow problems. CFD becomes an important engineering tool because it can provide clear insight into many fluid flow phenomena and produce extremely large volumes of results with inexpensive operating cost. CFD is very powerful and spans a wide range of engineering application areas e.g., aerodynamics of aircraft and vehicles, hydrodynamics of ships, mixing and separation in chemical processes, etc. [3].

2.1.1 CFD processing

Generally, CFD program contains three main processes, including pre-processor, solver, and post-processor.

Pre-processor

This step consists of the input of flow problem to a CFD program, such as definition of the computational domain, grid generation, selection of the physical and chemical phenomena, definition of material properties, etc.

Solver

There are three distinct streams of numerical solution technique, including finite difference method, finite element method, and finite volume methods. Generally, the solver performs the following steps,

- Approximation of unknown flow variables by simple function.
- Transform the PDEs into algebraic equation. This step is called discretization.
- Solution of the algebraic equations.

Post-processor

Post-processor contains versatile data visualization tools, such as geometry and grid display, vector plot, line and shaded contour plots, etc. CFD processing can be summarized as a diagram, which shown in Figure 2.1.

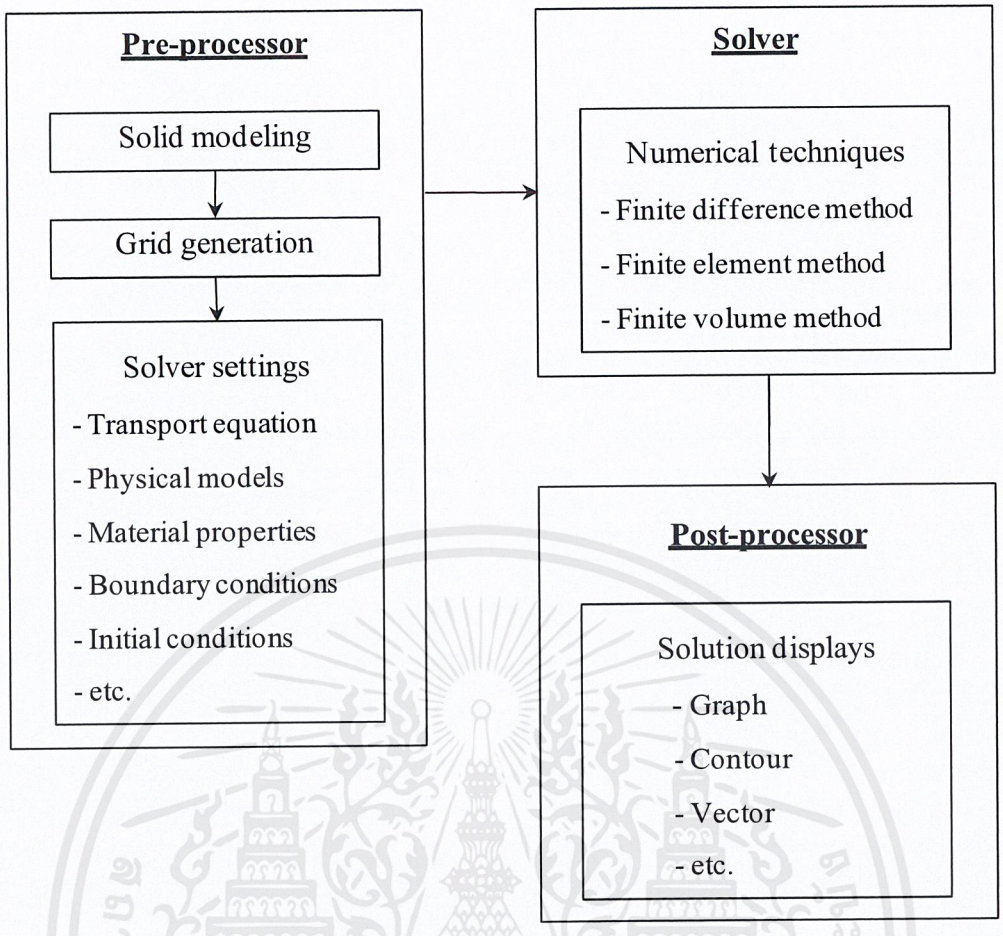

Figure 2.1 CFD processing diagram

2.1.2 Finite volume method

Finite volume method is numerical solution technique. This method was originally developed as a special finite difference formulation. Finite volume method consists of the following steps,

- Integration of fluid flow governing equations over control volume.
- Discretization involves the substitution of a variety of finite-difference-type approximations in the integrated equation, including convection term, diffusion term and source term. This converts the integral equations into a set of algebraic equations.
- Solution of the algebraic equations by an iterative method.

2.2 Governing equations

The fluid problems are usually governed by three fundamental physical equations, including the conservation of mass, the Newton's second law of motion, and the first law of thermodynamics.

2.2.1 Mass conservation equation

The conservation of mass states that mass may be neither created nor destroyed. The mass conservation equation or continuity equation is given by

$$\frac{\partial \rho}{\partial t}+\frac{\partial}{\partial x}(\rho u)+\frac{\partial}{\partial y}(\rho v)+\frac{\partial}{\partial z}(\rho w)=0 \tag{2.1}$$

or

$$\frac{\partial \rho}{\partial t}+\nabla\cdot(\rho \mathbf{U})=0 \tag{2.2}$$

where $\mathbf{U}$ is the velocity vector in cartesian coordinate, and given by

$$\mathbf{U}=u\mathbf{i}+v\mathbf{j}+w\mathbf{k}$$

where $\mathbf{i}$, $\mathbf{j}$, and $\mathbf{k}$ are the unit vectors along x, y, and z axes, respectively.

2.2.2 Momentum equations

The Newton's second law of motion states that the time rate of change of momentum of a system is equal to the net force acting on the system and takes place in the direction of the net force. The three momentum conservation equations are given by

x-component:

$$\rho\frac{Du}{Dt}=\frac{\partial}{\partial t}(\rho u)+\nabla\cdot(\rho u\mathbf{U})=-\frac{\partial p}{\partial x}+\frac{\partial \tau_{xx}}{\partial x}+\frac{\partial \tau_{yx}}{\partial y}+\frac{\partial \tau_{zx}}{\partial z}+S_{Mx} \tag{2.3}$$

y-component:

$$\rho\frac{Dv}{Dt}=\frac{\partial}{\partial t}(\rho v)+\nabla\cdot(\rho v\mathbf{U})=-\frac{\partial p}{\partial y}+\frac{\partial \tau_{xy}}{\partial x}+\frac{\partial \tau_{yy}}{\partial y}+\frac{\partial \tau_{zy}}{\partial z}+S_{My} \tag{2.4}$$

z-component:

$$\rho\frac{Dw}{Dt}=\frac{\partial}{\partial t}(\rho w)+\nabla\cdot(\rho w\mathbf{U})=-\frac{\partial p}{\partial z}+\frac{\partial \tau_{xz}}{\partial x}+\frac{\partial \tau_{yz}}{\partial y}+\frac{\partial \tau_{zz}}{\partial z}+S_{Mz} \qquad (2.5)$$

2.3 Turbulence and k-epsilon turbulence model

Fluid flow pattern, including laminar, transition, and turbulent can be identified by Reynolds number (Re). The Reynolds number can be defined as the relative importance of inertia forces and viscous forces. In experiments on fluid systems it is observed that at values below the critical Reynolds number (Re_{crit}), the flow is smooth and adjacent layers of fluid slide past each other in an orderly fashion. This regime is called laminar flow. At values above Re_{crit}, a complicated series of events takes place which eventually leads to a radical change of the flow character. In the final state the flow behavior is random and chaotic even with constant imposed boundary conditions. This regime is called turbulent flow [4].

2.3.1 Characteristics of the turbulent flow

- Highly unsteady: The velocity is a function of time. The typical point velocity measurement might exhibit the form shown in Figure 2.2.

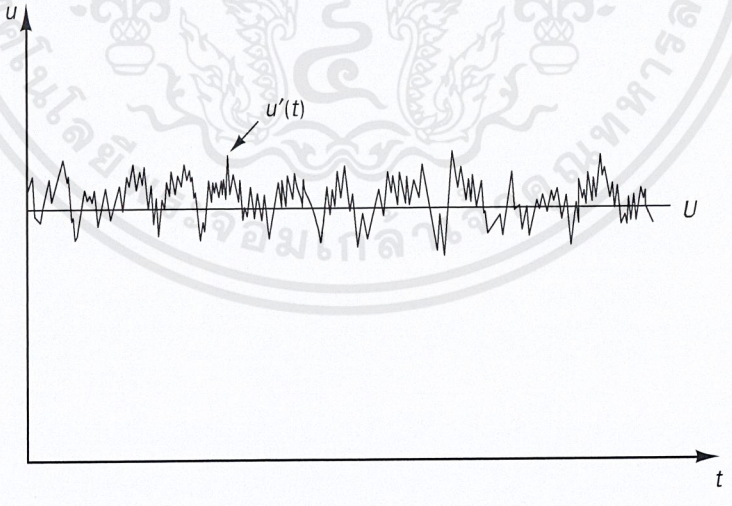

Figure 2.2 Typical point velocity in turbulent flow [4]

- Irregularity: It is another characteristic which makes the deterministic approach to turbulence problems impossible. One should relay on statistical approach.

- Diffusivity: If the flow pattern is random but does not exhibit spreading of velocity fluctuations through the surrounding fluid then the flow is not turbulent. This characteristic of turbulence causes rapid mixing and increased rates of momentum, heat, and mass transfer.
- Three dimensional: Turbulence is three dimensional and rotational.
- Dissipative: The turbulent flows are always dissipative.
- Higher Reynolds number: Turbulence in the fluid flow always occurs at high Reynolds numbers.

2.3.2 Reynolds average Navier-Stokes equations (RANS)

According to irregular characteristic of turbulent flow, the computations based on the complete description of all fluid particles motion are impossible. However, the computations of turbulent flow can be solved by using statistical approach. The instantaneous flow property (φ) is decomposed into its time-averaged ($\overline{\varphi}$) and fluctuating quantities (φ') as shown in equation (2.6).

$$\varphi(t) = \overline{\varphi} + \varphi'(t) \tag{2.6}$$

This process is called Reynolds decomposition, which first proposed by Osborne Reynolds. The definition of time-average of flow property (φ) and time-average of fluctuation property (φ') are given by

$$\overline{\varphi} = \frac{1}{\Delta t}\int_0^{\Delta t} \varphi(t)dt \tag{2.7}$$

$$\overline{\varphi'} = \frac{1}{\Delta t}\int_0^{\Delta t} \varphi'(t)dt \equiv 0 \tag{2.8}$$

Regarding to Reynolds decomposition, pressure, velocity vector, and three velocity components, including x-, y-, and z-component can be expressed as

$$p(t) = \overline{p} + p'(t) \tag{2.9}$$

$$\mathbf{U}(t) = \overline{\mathbf{U}} + \mathbf{U}'(t) \tag{2.10}$$

$$u(t) = \bar{u} + u'(t) \tag{2.11}$$

$$v(t) = \bar{v} + v'(t) \tag{2.12}$$

$$w(t) = \bar{w} + w'(t) \tag{2.13}$$

The effects of fluctuations on mean flow can be investigated by replace the equations (2.9) to (2.13) into governing equations and apply time-average of flow property as shown in equations (2.7) and (2.8).

The compressible continuity equation for the mean flow is given by

$$\frac{\partial \rho}{\partial t} + \frac{\partial}{\partial x}\left(\rho\bar{u}\right) + \frac{\partial}{\partial y}\left(\rho\bar{v}\right) + \frac{\partial}{\partial z}\left(\rho\bar{w}\right) = 0 \tag{2.14}$$

or

$$\frac{\partial \rho}{\partial t} + \nabla \cdot \left(\rho\bar{\mathbf{U}}\right) = 0 \tag{2.15}$$

The time-average momentum equations for compressible fluid with constant viscosity are given by

x-component:

$$\frac{\partial}{\partial t}\left(\rho\bar{u}\right) + \frac{\partial}{\partial x}\left(\rho\bar{u}^2\right) + \frac{\partial}{\partial y}\left(\rho\bar{u}\bar{v}\right) + \frac{\partial}{\partial z}\left(\rho\overline{uw}\right)$$

$$= -\frac{\partial \bar{p}}{\partial x} + \mu\frac{\partial^2 \bar{u}}{\partial x^2} + \mu\frac{\partial^2 \bar{u}}{\partial y^2} + \mu\frac{\partial^2 \bar{u}}{\partial z^2}$$

$$+\left[-\frac{\partial}{\partial x}\left(\rho\overline{(u')^2}\right) - \frac{\partial}{\partial y}\left(\rho\overline{u'v'}\right) - \frac{\partial}{\partial z}\left(\rho\overline{u'w'}\right)\right] + S_{Mx} \tag{2.16}$$

or

$$\frac{\partial}{\partial t}\left(\rho\bar{u}\right) + \nabla \cdot \left(\rho\bar{u}\bar{\mathbf{U}}\right) = -\frac{\partial \bar{p}}{\partial x} + \mu\nabla^2\bar{u}$$

$$+\left[-\frac{\partial}{\partial x}\left(\rho\overline{(u')^2}\right) - \frac{\partial}{\partial y}\left(\rho\overline{u'v'}\right) - \frac{\partial}{\partial z}\left(\rho\overline{u'w'}\right)\right] + S_{Mx} \tag{2.17}$$

y-component:

$$\frac{\partial}{\partial t}(\rho\bar{v})+\frac{\partial}{\partial x}(\rho\bar{v}\bar{u})+\frac{\partial}{\partial y}(\rho\bar{v}^2)+\frac{\partial}{\partial z}(\rho\bar{v}\bar{w})$$

$$=-\frac{\partial\bar{p}}{\partial y}+\mu\frac{\partial^2\bar{v}}{\partial x^2}+\mu\frac{\partial^2\bar{v}}{\partial y^2}+\mu\frac{\partial^2\bar{v}}{\partial z^2}$$

$$+\left[-\frac{\partial}{\partial x}(\rho\overline{u'v'})-\frac{\partial}{\partial y}(\rho\overline{(v')^2})-\frac{\partial}{\partial z}(\rho\overline{v'w'})\right]+S_{My} \qquad (2.18)$$

or $$\frac{\partial}{\partial t}(\rho\bar{v})+\nabla\cdot(\rho\bar{v}\bar{\mathbf{U}})=-\frac{\partial\bar{p}}{\partial y}+\mu\nabla^2\bar{v}$$

$$+\left[-\frac{\partial}{\partial x}(\rho\overline{u'v'})-\frac{\partial}{\partial y}(\rho\overline{(v')^2})-\frac{\partial}{\partial z}(\rho\overline{v'w'})\right]+S_{My} \qquad (2.19)$$

z-component:

$$\frac{\partial}{\partial t}(\rho\bar{w})+\frac{\partial}{\partial x}(\rho\bar{w}\bar{u})+\frac{\partial}{\partial y}(\rho\bar{w}\bar{v})+\frac{\partial}{\partial z}(\rho\bar{w}^2)$$

$$=-\frac{\partial\bar{p}}{\partial z}+\mu\frac{\partial^2\bar{w}}{\partial x^2}+\mu\frac{\partial^2\bar{w}}{\partial y^2}+\mu\frac{\partial^2\bar{w}}{\partial z^2}$$

$$+\left[-\frac{\partial}{\partial x}(\rho\overline{u'w'})-\frac{\partial}{\partial y}(\rho\overline{v'w'})-\frac{\partial}{\partial z}(\rho\overline{(w')^2})\right]+S_{Mz} \qquad (2.20)$$

or $$\frac{\partial}{\partial t}(\rho\bar{w})+\nabla\cdot(\rho\bar{w}\bar{\mathbf{U}})=-\frac{\partial\bar{p}}{\partial z}+\mu\nabla^2\bar{w}$$

$$+\left[-\frac{\partial}{\partial x}(\rho\overline{u'w'})-\frac{\partial}{\partial y}(\rho\overline{v'w'})-\frac{\partial}{\partial z}(\rho\overline{(w')^2})\right]+S_{Mz} \qquad (2.21)$$

The equations (2.16) to (2.21) are called the Reynolds equation. There are new terms arise in equations (2.16) to (2.21), which are associated with turbulent velocity fluctuations. These extra turbulent stresses, which describe the diffusive nature of turbulence, are called Reynolds stresses.

For convenience, the new notation of these Reynolds stresses can be expressed as

$$\bar{\tau}_{ij}^{(t)} = -\rho\overline{u_i' u_j'} = \mu_t\left(\frac{\partial \overline{u_i}}{\partial x_j} + \frac{\partial \overline{u_j}}{\partial x_i}\right) \tag{2.22}$$

where μ_t is turbulent viscosity or eddy viscosity, which usually depends strongly on position.

The relation in equation (2.22) was first postulated by Boussinesq in 1877. Thus, equations (2.17), (2.19), and (2.21) become

x-component:

$$\frac{\partial}{\partial t}\left(\rho\bar{u}\right) + \nabla\cdot\left(\rho\bar{u}\overline{\mathbf{U}}\right) = -\frac{\partial \bar{p}}{\partial x} + \mu_{eff}\nabla^2\bar{u} + S_{Mx} \tag{2.23}$$

y-component:

$$\frac{\partial}{\partial t}\left(\rho\bar{v}\right) + \nabla\cdot\left(\rho\bar{v}\overline{\mathbf{U}}\right) = -\frac{\partial \bar{p}}{\partial y} + \mu_{eff}\nabla^2\bar{v} + S_{My} \tag{2.24}$$

z-component:

$$\frac{\partial}{\partial t}\left(\rho\bar{w}\right) + \nabla\cdot\left(\rho\bar{w}\overline{\mathbf{U}}\right) = -\frac{\partial \bar{p}}{\partial z} + \mu_{eff}\nabla^2\bar{w} + S_{Mz} \tag{2.25}$$

where μ_{eff} is the effective viscosity coefficient which is expressed as

$$\mu_{eff} = \mu + \mu_t \tag{2.26}$$

2.3.3 k-epsilon turbulence model

The k-epsilon model is one of the most common turbulence models which includes two extra transport equations to represent the turbulent properties of the flow. This model was proposed by Launder and Spalding [5]. The first transport equation is transport equation of turbulent kinetic energy (k) and the second one is transport

equation of dissipation rate of turbulent kinetic energy (ε). Two transport equations can be shown in equation (2.27) and (2.28), respectively.

k-transport equation:

$$\frac{\partial}{\partial t}(\rho k)+\frac{\partial}{\partial x_i}\left(\rho k\overline{u_i}\right)=\frac{\partial}{\partial x_j}\left[\left(\mu+\frac{\mu_t}{\sigma_k}\right)\frac{\partial k}{\partial x_j}\right]+G_k+G_b-\rho\varepsilon-Y_M+S_k \qquad (2.27)$$

ε -transport equation:

$$\frac{\partial}{\partial t}(\rho\varepsilon)+\frac{\partial}{\partial x_i}\left(\rho\varepsilon\overline{u_i}\right)=\frac{\partial}{\partial x_j}\left[\left(\mu+\frac{\mu_t}{\sigma_\varepsilon}\right)\frac{\partial\varepsilon}{\partial x_j}\right]+C_{1\varepsilon}\frac{\varepsilon}{k}\left(G_k+C_{3\varepsilon}G_b\right)-C_{2\varepsilon}\rho\frac{\varepsilon^2}{k}+S_\varepsilon \qquad (2.28)$$

where $\mu_t=\rho C_\mu\dfrac{k^2}{\varepsilon}$, $G_k=-\rho\overline{u_i'u_j'}\dfrac{\partial\overline{u_j}}{\partial x_i}$, $G_b=\beta g_i\dfrac{\mu_t}{\mathrm{Pr}_t}\dfrac{\partial T}{\partial x_i}$, $Y_M=2\rho\varepsilon M_t^2$,

$C_{3e}=\tanh\left|\dfrac{v}{u}\right|$ and the model constants in these equations are shown in Table 2.1.

Table 2.1 Model constant for k-epsilon turbulence model [6]

$C_{1\varepsilon}$	$C_{2\varepsilon}$	C_μ	σ_k	σ_ε
1.44	1.92	0.09	1.0	1.3

2.4 Flow in noncircular channels

Although the round pipe is a very common conveyance for flowing fluids, ducts of other cross sections are commonly encountered (see Figure 2.3) is shows a ducting system of the type frequently used for distributing conditioned air for either heating or cooling residential spaces.

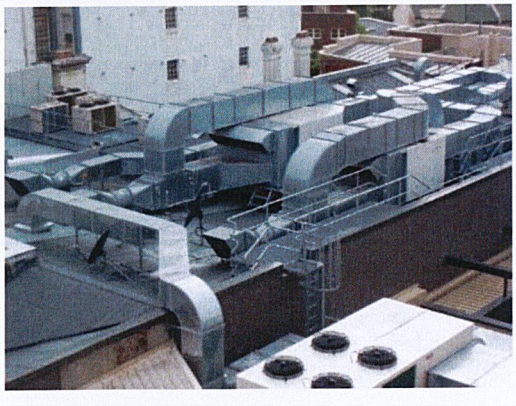

Figure 2.3 Complex ducting system involving noncircular ducts

If a duct is sufficiently long, a fully developed flow will occur regardless of the shape of the duct cross section [7]. The conditions for fully developed flow are the same both for round pipes and non-circular ducts. They are a pressure drop characterized by a constant slope and velocity profiles which maintain a given shape. The magnitude of the pressure gradient and the shape of the velocity profile depend on the nature of the duct cross section. Furthermore, the distance from the duct inlet at which fully developed conditions are first encountered also depends on the cross-sectional shape. Two commonly encountered non-circular cross sections are the rectangular and the annular ducts which are pictured in Figure 2.4.

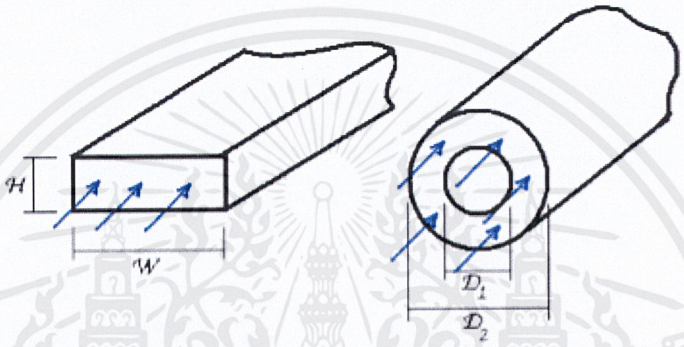

Figure 2.4 Noncircular ducts, rectangular duct and annular

It is clear from Figure 2.4 that more than one dimension is needed for the description of the cross-sectional shapes of non-circular ducts. This fact leads to a dilemma with regard to the Reynolds number. In the definition of the Reynolds number, there is space to accommodate a single dimension. For a round pipe, that dimension is clearly the diameter. The difficulty with regard to the Reynolds number for non-circular ducts is the need to find a single dimension that characterizes the non-circular cross section.

Guidance for the selection of the appropriate single dimension can be taken by consideration of Newton's Second Law for fully developed flow in pipes and ducts. To implement the discussion, Figure 2.5 is shown as a control volumes specific to circular and non-circular ducts. For fully developed flow, the rate at which x-directed momentum enters the control volume is precisely equal to the rate at which the x-directed momentum leaves the control volume. Therefore, the application of Newton's second law reduces to a force balance between the pressure and shear forces.

Figure 2.5 Control volumes for the analysis of
fully developed flow in circular pipes and non-circular ducts

For the case of the circular cross section, equation 2.29 expresses the fully developed force balance.

$$\frac{dp}{dx} = \frac{4\tau_w}{D} \tag{2.29}$$

On the other hand, for the force balance for the case of the non-circular cross section, it is necessary to recognize that the resulting skewed velocity profile gives rise to a wall shear stress that varies around the circumference. For the execution of the force balance, it is convenient to let $\bar{\tau}_w$ denote the average wall shear. With this notation, the force balance for the non-circular case is:

$$-\frac{dp}{dx} = \frac{\bar{\tau}_w C}{A} \tag{2.30}$$

To bring the force balances of equation 2.29 and 2.30 into congruence,

$$\frac{4}{D} = \frac{C}{A} \tag{2.31}$$

or,

$$D = \frac{4A}{C} \tag{2.32}$$

The quantity D represented by equation 2.32 is the equivalent diameter of a round pipe which yields the same force balance as that for a non-circular duct. It is common practice to denote this quantity as *the hydraulic diameter* (D_H), so that:

$$D_H = \frac{4A}{C} \tag{2.33}$$

It is important to note the result of applying this definition to a round pipe, which gives

$$D_H = \frac{4\pi\frac{D^2}{4}}{\pi D} = D \tag{2.34}$$

Therefore, the definition of the hydraulic diameter is equally applicable to circular and noncircular ducts.

For the rectangular duct that is pictured in Figure 2.4,

$$D_H = \frac{4HW}{2(H+W)} = \frac{2H}{1+\frac{H}{W}} \tag{2.35}$$

The quantity W/H is called the *aspect ratio*. For ducts that are wide, relative to their height, the aspect ratio approaches infinity, and H/W approaches zero. Such ducts are called *parallel-plate channels* and are characterized by hydraulic diameters $D_H = 2H$.

2.5 Flow past immersed objects

2.5.1 Lift and drag concepts

When anybody moves through a fluid, an interaction between the body and the fluid occurs; this effect can be described in terms of the forces at the fluid body interface. This can be described in terms of the stresses wall shear stresses, due to viscous effects and normal stresses due to the pressure (p) [8]. Typical shear stress and pressure distributions are shown in Figure 2.6(a) and 2.6(b). Both τ_w and p vary in magnitude and direction along the surface. It is often useful to know the detailed distribution of shear stress and pressure over the surface of the body, although such information is difficult to obtain. Many times, however, only the integrated or resultant effects of these distributions are needed. The resultant force in the direction of the upstream velocity is termed the drag (F_D), and the resultant force normal to the upstream velocity is termed the lift (F_L)as is indicated in Figure 2.6(c). The resultant of the shear stress and pressure distributions can be obtained by integrating the effect of these two quantities on the body surface as is indicated in Fig. The x and y components of the fluid force on the small area element dA are:

$$dF_x = (pdA)\cos\theta + (\tau_w dA)\sin\theta \tag{2.36}$$

$$dF_y = -(pdA)\sin\theta + (\tau_w dA)\cos\theta \tag{2.37}$$

The widely-used alternative is to define dimensionless lift and drag coefficients and determine their approximate values by means of either a simplified analysis, some numerical technique, or an appropriate experiment. The *lift coefficient*, and *drag coefficient*, are defined as:

$$C_D = \frac{F_D}{\frac{1}{2}\rho U^2 A}, \qquad C_L = \frac{F_L}{\frac{1}{2}\rho U^2 A} \tag{2.38}$$

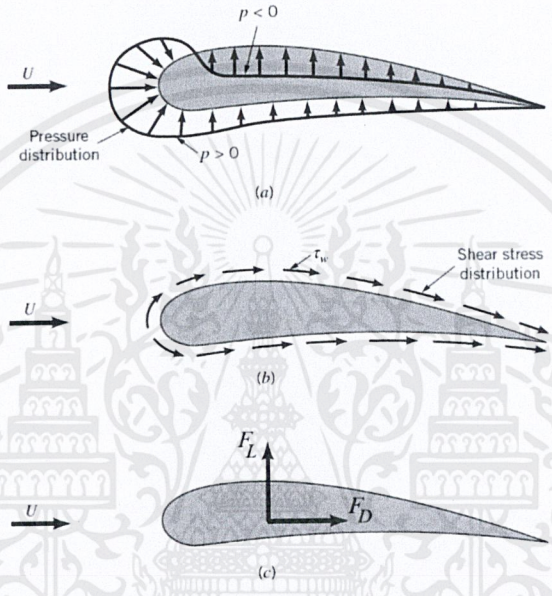

Figure 2.6 Forces from surrounding fluid (a) pressure force, (b) viscous force and (c) resultant force

$$F_D = \int_A dF_x = \int_A p\cos\theta dA + \int_A \tau_w \sin\theta\, dA \tag{2.39}$$

$$F_L = \int_A dF_y = -\int_A p\sin\theta dA + \int_A \tau_w \cos\theta\, dA \tag{2.40}$$

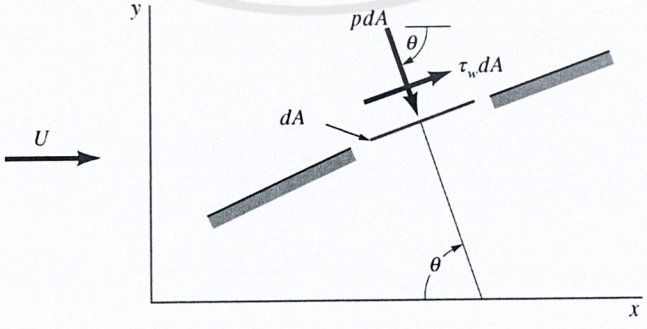

Figure 2.7 Pressure and shear forces on a small element of the surface of a body

where A is taken to be *frontal area*- projected are seen by a person looking toward the object from a direction parallel to the upstream velocity, U or as *planform area* - the projected area seen by an observer looking toward the object from a direction normal to the upstream velocity. Classification of body shape can be made depending on whether the body is streamlined or blunt. In general, *streamlined bodies* (i.e., airfoils, racing cars, etc.) have little effect on the surrounding fluid, compared with the effect that *blunt bodies* (i.e., parachutes, buildings, etc.) have on the fluid.

2.5.2 Friction drag

Friction drag (F_F) is that part of the drag that is due directly to the shear stress, on the object. It is a function of not only the magnitude of the wall shear stress, but also of the orientation of the surface on which it acts. This is indicated by the factor $\tau_w \sin\theta$ in equation 2.39. If the surface is parallel to the upstream velocity, the entire shear force contributes directly to the drag. This is true for the flat plate parallel to the flow. If the surface is perpendicular to the upstream velocity, the shear stress contributes nothing to the drag.

The friction drag on a flat plate of width b and length l oriented parallel to the upstream flow can be calculated from

$$F_D = C_{D_f} \frac{1}{2} \rho U^2 bl \qquad (2.41)$$

where C_{D_f} is the friction drag coefficient. The value of C_{D_f} is given as a function of Reynolds number, $Re_l = \rho Ul/\mu$, and relative surface roughness, ε/l. The precise determination of the shear stress along the surface of a curved body is quite difficult to obtain.

2.5.3 Pressure drag

Pressure drag, is that part of the drag that is due directly to the pressure (p) on an object. It is often referred to as *form drag* because of its strong dependency on the shape or form of the object. Pressure drag is a function of the magnitude of the pressure and the orientation of the surface element on which the pressure force acts. For example, the pressure force on either side of a flat plate parallel to the flow may be very large, but it does not contribute to the drag because it acts in the direction normal to the upstream velocity. On the other hand, the pressure force on a flat plate normal to the flow provides the entire drag. If the viscosity were zero, the pressure drag on any shaped object (symmetrical or not) in a steady flow would be zero.

There perhaps would be large pressure forces on the front portion of the object, but there would be equally large (and oppositely directed) pressure forces on the rear portion. If the viscosity is not zero, the net pressure drag may be nonzero because of boundary layer separation.

2.6 Developing and fully developed flow

2.6.1 The entrance region

Flows completely bounded by solid surfaces are called internal flows. Thus, internal flows include flows through pipes, ducts, nozzles, diffusers, valves and fittings. In many practical cases the flow in pipes is not fully developed, but rather in the process of developing and hence eventually reaching the fully developed state.

Consider a fluid entering a circular pipe at a uniform velocity. Because of the no-slip condition, the fluid particles in the layer in contact with the surface of the pipe come to a complete stop. This layer also causes the fluid particles in the adjacent layers to slow down gradually as a result of friction. To make up for this velocity reduction, the velocity of the fluid at the midsection of the pipe has to increase to keep the mass flow rate through the pipe constant. As a result, a velocity gradient develops along the pipe.

The region of the flow in which the effects of the viscous shearing forces caused by fluid viscosity are felt is called the *velocity boundary layer* or just the *boundary layer* [10]. The hypothetical boundary surface divides the flow in a pipe into two regions, *the boundary layer region*, in which the viscous effects and the velocity changes are significant, and the *irrotational (core) flow region*, in which the frictional effects are negligible and the velocity remains essentially constant in the radial direction.

The thickness of this boundary layer increases in the flow direction until the boundary layer reaches the pipe center and thus fills the entire pipe, as shown in Figure 2.8. The region from the pipe inlet to the point at which the boundary layer merges at the centerline is called the *entrance region*, and the length of this region is called the *entrance length* (L_e). Flow in the entrance region is called *developing flow* since this is the region where the velocity profile develops. The region beyond the entrance region in which the velocity profile is fully developed and remains unchanged is called the *fully developed region*. The flow is said to be *fully developed*.

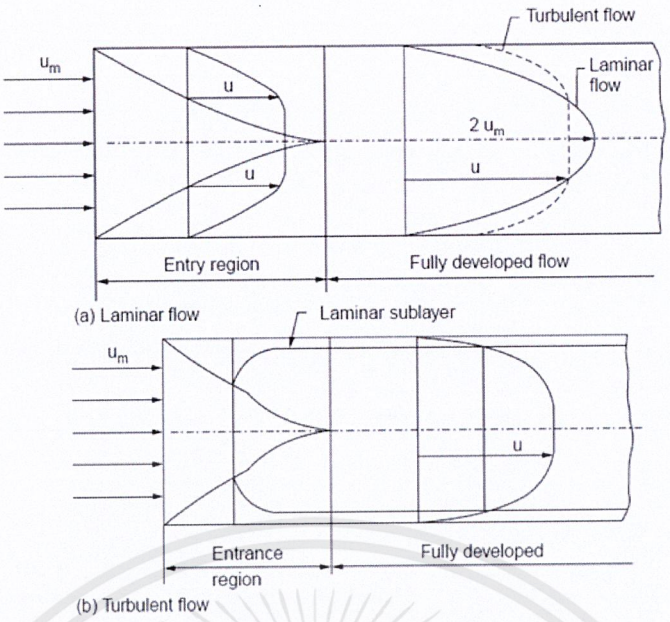

Figure 2.8 The development of the velocity boundary layer in a pipe

The velocity profile in the fully developed region is parabolic in laminar flow and somewhat flatter (or fuller) in turbulent flow due to eddy motion and more vigorous mixing in the radial direction. The time-averaged velocity profile remains unchanged when the flow is fully developed, and thus:

$$\frac{\partial u(r,x)}{\partial x} = 0 \quad \rightarrow \quad u = u(r) \tag{2.42}$$

2.6.2 The entrance length

The difference between laminar and turbulent flow in a pipe applies only to the fully developed flow condition. In the development zone, the core flow is irrotational either laminar or turbulent. The flow in the boundary-layer is laminar or turbulent. If the fully developed flow is laminar (Re < 2,300), the boundary-layer is laminar, likewise if the fully developed flow is turbulent (Re ≥ 4,000), the boundary-layer is laminar near the pipe entrance, undergoes transition and is turbulent as it approaches the fully developed condition [11]

and, thus:

$$\frac{L_e}{D} = f(Re) \tag{2.43}$$

where D is diameter

The function f is different for laminar and turbulent flow. Analytic and experimental investigations have shown the validity of the following correlations [9].

Laminar flow $$\frac{L_e}{D} \approx 0.06Re \quad (2.44)$$

and

Turbulent flow $$\frac{L_e}{D} \approx 4.4(Re)^{\frac{1}{6}} \quad (2.45)$$

The longest practical entrance length corresponds to laminar flow with $Re \approx$ 2,300

$$\left(\frac{L_e}{D}\right)_{max} \approx 140 \quad (2.46)$$

In many engineering pipe flows, Re is between 10^4 to 10^5. For the turbulent flow, the entrance length is found experimentally to be considerably less than those require for laminar flow, due to the large amount of mixing caused by the turbulence. It is found in experimentally that the wall shear stress and axial pressure gradient attain their fully developed mean values in entrance length in smooth pipe of less than 25 diameters. However, the detailed structure of the turbulence requires considerably longer entrance length to become full developed [12], typical engineering flow:

$$\frac{L_e}{D} \approx 25 \quad (2.47)$$

With many pipes in engineering applications being hundreds or thousands of diameters long, the flow is fully developed over most of their lengths.

2.7 Jet flow

Jet flow is one of shear flow which have sources of flow in momentum. Fluid flows through a channel or nozzle to another static fluid cause a shear layer between two fluids. Due to the difference in velocity between the jet and the surrounding fluid, it causes an eddy motion at the shear layer then entrainment and mixing the fluid. Therefore, the jet flow has been applied extensively [11].

In general, the jet flow classification is divided with injection conditions, are free jet, wall jet and surface jet. All three types of jet open up to the fluid, near or close to the solid surface and near or at the skin surface, respectively. (see Figure 2.9)

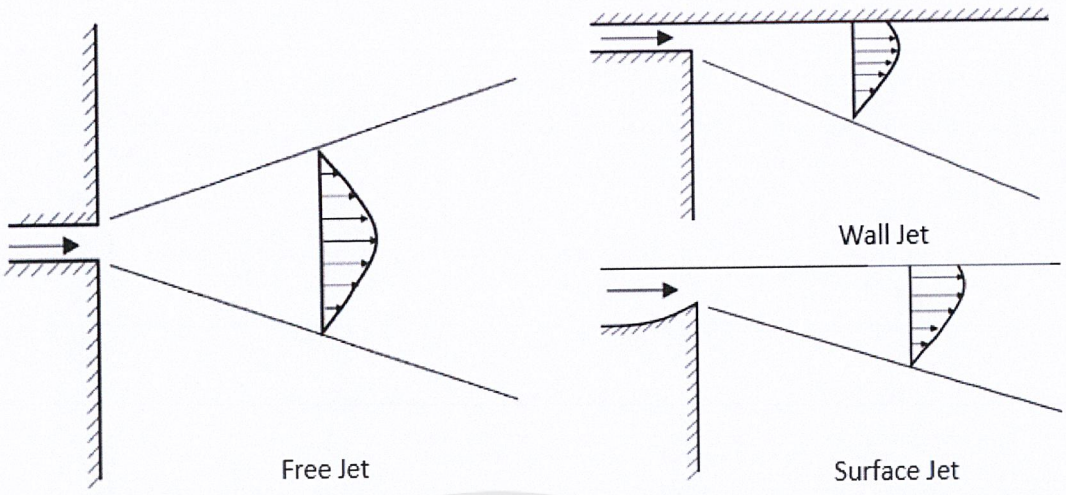

Figure 2.9 Jet flow classification

According to Figure 2.9, it will be seen that the characteristics of each type of jet are not the same. Free jet is symmetrical with centerline of the jet because it is not influenced by side wall. Therefore, the free shear layer is formed between the jet and surrounding fluid is equally influenced in all directions. Also, free jet can entrain mass of fluid in all direction, it is remarkable feature of this jet. The characteristic of wall jet is asymmetrical because one side of the jet is attached the wall, so the shear layer is divided into two areas. At the wall area is a boundary layer and free shear layer at the surrounding fluid, so the wall jet can entrain mass of fluid in all direction except the direction which attached the wall. For the surface jet, a characteristic of the jet is an asymmetric as well. The one side of the jet exposed to the open surface, the shear layer is divided into two areas. The shear layer is free shear layer but different in that the jet are sheared with different types of fluids. The top of the jet being sheared with air, the rest is sheared with the surrounding fluid. This allows the mass of the jet to entrain both air and fluid into the center of the jet.

The jet flow properties are controlled by a dimensionless variable called Reynold Number (Re). Which is the relations between inertia force and viscous force.

$$Re = \frac{Inertia\ forces}{Viscous\ forces} = \frac{\rho\bar{v}^2}{\mu\bar{v}/L_c} = \frac{\rho\bar{v}L_c}{\mu} = \frac{\bar{v}L_c}{v} \qquad (2.48)$$

where $\bar{v}$ is average velocity

L_c is characteristic length

v is kinematic viscosity

2.8 Literature reviews

Before the details of the present study are given, a brief of review of the previous works on experimental study and numerical approach for the flow past an obstacle with infinite extent and also for the flow separation of internal flow are first made.

The phenomenon of a fluid flow pass an obstacle and associated resistance of fluids, must have been one of the oldest experiments. From an analytical point of view, it is also one of the most difficult problems in fluid mechanics. Rayleigh, in his 1876 paper [13], observed that "there is no part of hydrodynamics more perplexing to the student than that which treats of the resistance of fluids." And presented the theory of *discontinuous* motion to predict a drag coefficient for an inclined flat plate in an infinite flow flied.

Cheng and Chen, 1987 [14], studied on finite analytic numerical solutions of incompressible flow past inclined axisymmetric bodies. The Navier-Stokes equations are solved by FANS-3DEF which based on the finite analytic method on the body-fitted coordinate system with modified SIMPLER algorithm.

Cherdron, Durst and Whitelaw, 1978 [15], observed experiments on asymmetric separation of internal laminar flows. This asymmetry occurs in spite of symmetric inlet profiles and the symmetry of the test-section geometry. The results suggest that the origin of the asymmetry is related to the shear layers and to coherent flow structures embedded in the random velocity fluctuation. Then structures exist in shear layers can interact with each other, yielding phenomena that dominate the flow characteristics.

Durst and Rastogi, 1979 [16], invested the flow visualization experiments of turbulent flows with separation and also used the finite difference solution procedures for calculating in the redevelopment region by the computer program GENMIX. The two-dimensional form of the continuity and the time-averaged Navier-Stokes equations were carried out to solve with both k-ε and three-equation k-ε-$\overline{u'v'}$ turbulence model. The calculation is compared with the measurements and demonstrate clearly that use of the three-equation model improves the calculated profiles further but not significantly and not offer worthwhile advantages over the two-equation k-ε turbulence model.

Wattananusorn, 1997 [2], the studied of the phenomena of air flow past the parallel inclined flat plates in a square duct through numerical solution by using computational fluid dynamics technique. A computer program called PHOENICS, is adopted to solve for three-dimensional steady turbulent flow under finite volume method. The incompressible, ensemble-averaged and Navier-Stokes equations were carried out to solve with k-ε turbulence model with Boussinesq's eddy viscosity assumption. The predictions show that the development length extends when the number of flat plates decreases, however, such length is shortened when the inclination of flat plates becomes smaller.

CHAPTER III

RESEARCH METHODOLOGY

This research was designed to simulate damper in rectangular duct into two parts together.

1.The accuracy of the rectangular duct model by validate with the experimental results for confirm that the model is created, it can be explaining flow phenomena well enough.

2.The influence of flow characteristic, type of damper and blade alignment to entrance length, then choose the suitable type of each characteristic flows.

3.1 The accuracy of the flow in a rectangular duct model

3.1.1 The geometry of the rectangular duct and damper

The model of damper and rectangular were created in 3D using GAMBIT 2.4.6, refer to the study of Wattananusorn,1997 [2]. The dimensions of rectangular duct are width (W) 0.6 meters, height (H) 0.3 meters and length (L) 40 meters (see Figure 3.1). Damper consists of 4 blades which are inclined 45°, and blades length (B.L.) 0.075 meters (see Figure 3.2). Then, assume the simulation is axisymmetric. The structural grid and finished of blank duct model are shown in Figure 3.3.

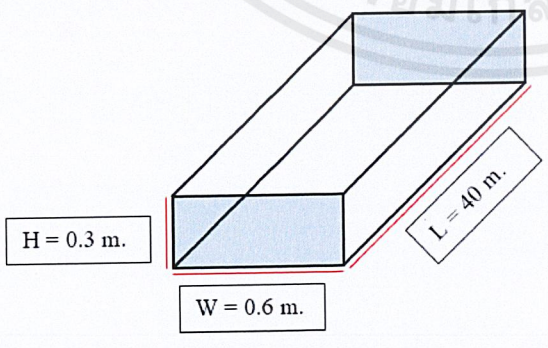

Figure 3.1 The structure of blank rectangular duct

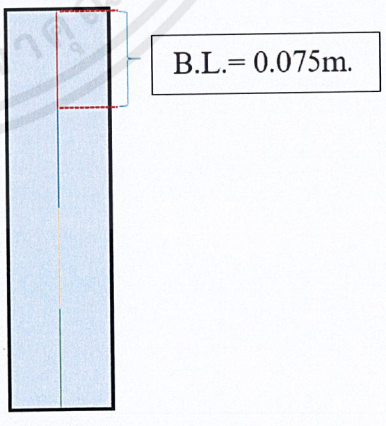

Figure 3.2 The damper with 4 blades

Figure 3.3 The numerical grid of blank rectangular duct

3.1.2 Configuration and modeling

In this research, the air flow under assumptions as steady state system, Newtonian fluid, constant fluid density and neglectful to body forces are simulated [2]. The settings are shown in the Table 3.1, 3.2, 3.3 and 3.4, respectively.

Table 3.1 Setting of boundary conditions

Boundaries	Boundary conditions
Inlet	Velocity-inlet are 1.5 m/s for turbulent flow and 0.0375 m/s for laminar flow in z-direction
Outlet	Pressure-outlet is 0 pascal (gauge)
Wall	Stationary wall and no slip condition
Damper blade	Stationary wall and no slip condition

Table 3.2 Setting of models

The region	Model
Laminar flow	Laminar
Turbulent flow	Standard k-epsilon

Table 3.3 Air properties

Properties	Values
Density	1.185 kg/m^3
Viscosity	1.7775×10^{-5} kg/m-s

Table 3.4 Setting of numerical schemes

Categories	Schemes
Pressure-velocity coupling scheme	SIMPLE
Gradient	Least squares cell based
Pressure	Standard
Momentum	Second order upwind
Turbulent kinetic energy	Second order upwind
Turbulent dissipation rate	Second order upwind

3.1.3 Grid independence study

The grid is important in simulation uses the computational fluid dynamics which need to be properly selected with phenomena in boundary. A small number of grid affects the simulation results that are incorrect. On the other hand, a large number of grid consumes calculation time without necessity. So, the study of grid independence is the ineluctable topic in this research.

In this research, grids number 341,850 cells, 650,332 cells, 1,379,096 cells, 1,631,700 cells and 3,523,360 cells are used. Grid distributions are shown in Table 3.5. After simulation, the results are collected and compared with the experimental results to find the suitable number of grid.

Table 3.5 Grid distribution in a blank rectangular duct

Grid numbers (cells)	Domains
341,850	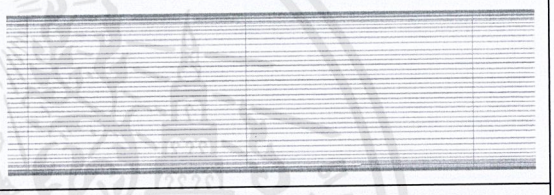
650,332	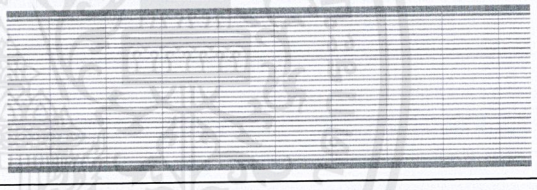
1,379,096	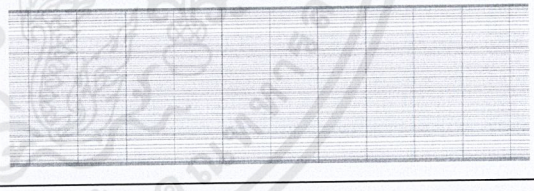
1,631,700	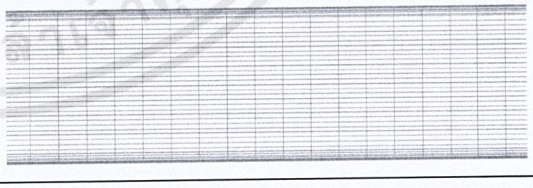
3,523,360	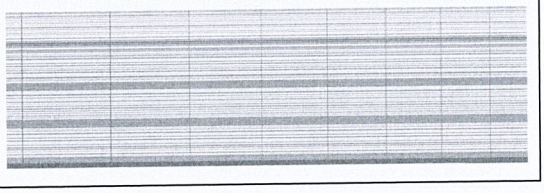

3.2 The parameters influencing to entrance length

In this research, flow characteristic including laminar flow and turbulent flow, damper's type including parallel-blade and opposed-blade and also blade alignment are used to compare the influence on entrance length. Figure 3.5-a and 3.5-b are both parallel-blade type but different in the blades alignment, then Figure 3.5-c and 3.5-d are the opposed-blade type. (see Figure 3.4).

- Parallel-blade

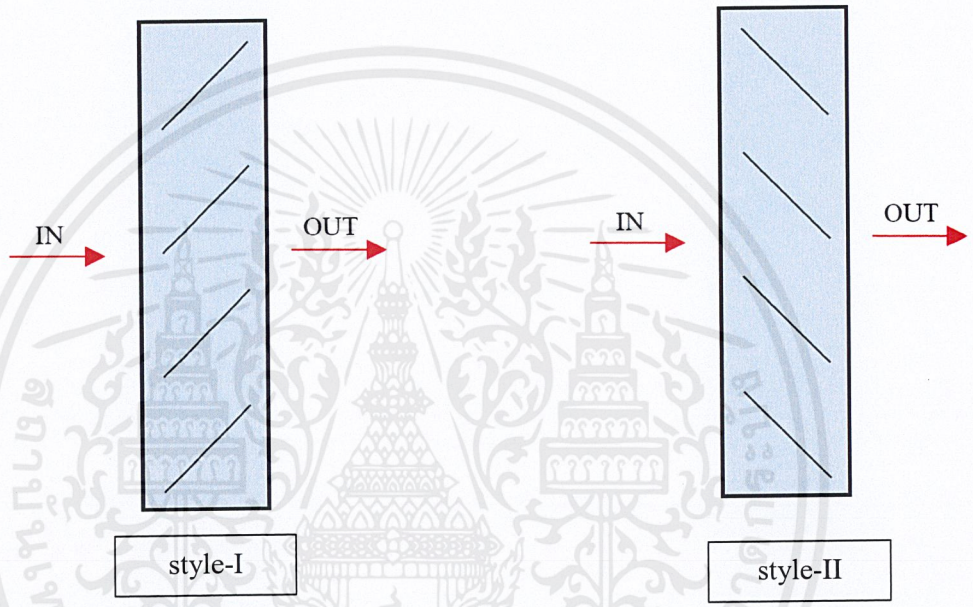

- Opposed-blade

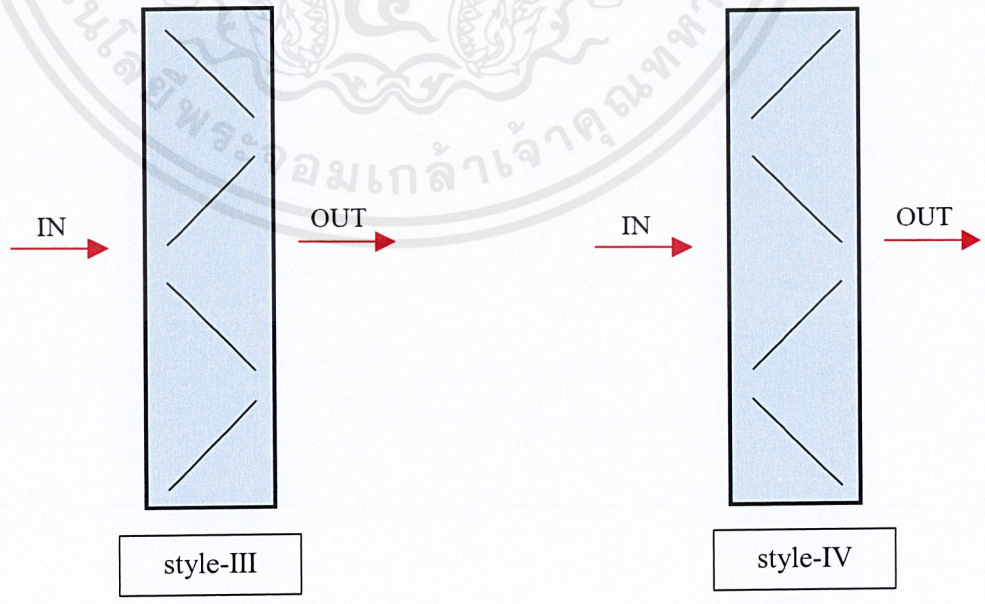

Figure 3.4 Damper sections in this research

CHAPTER IV
SIMULTION RESULTS AND DISCUSSION

4.1 Grid independence study and model validation

Size and resolution of grid is affect to the accuracy of results and calculation time. Then, the determination of grid independence is necessity this simulation. The simulation results of various grid numbers are shown in Table 4.1 that found when the number of grids increases, the ratio of entrance length to hydraulic diameter is not significance change, but time is increasingly too much.

Table 4.1 The simulation results of various grids

Grid (cells)	L_e/D	%Error	Calculation time (min)
Experiments	25	-	-
341,850	28	12	125
650,332	26	4	235
1,379,096	25	0	342
1,631,700	25	0	920
3,523,360	25	0	1,083

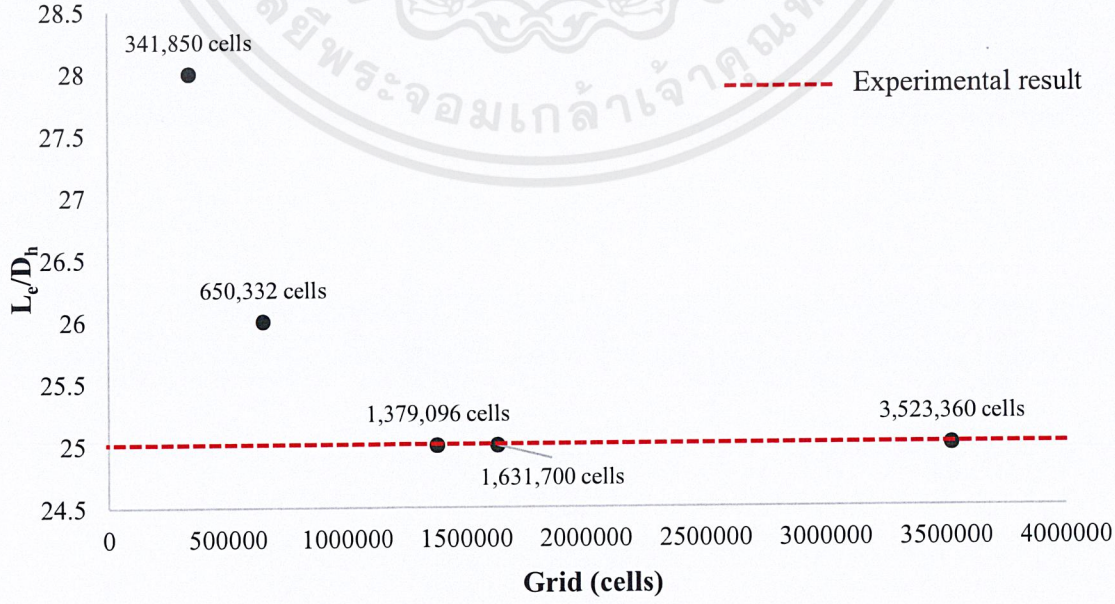

Figure 4.1 The number of grids to L_e/D_h of simulation

From Figure 4.1 is shown the relation between L_e/D_h and the number of grids which compared, that shown when grids have plenty more, work to be unchanged in prediction. Since the grid 1,379,096 cells, 1,631,700 cells and 3,523,360 that the results are not different, but the time to simulate has increased exponentially. From Table 4.1, the grid of 1,379,096 cells are appropriate to simulate the flow inside the rectangular duct and also consume simulation time in the right amount.

4.2 Entrance length in rectangular duct

In this research, the collecting data is plot five lines into the rectangular duct to get a velocity data along the length (see Figure 4.2). The definition of the criterion is that the fully developed flow region is promptly determined when the mean velocity of the last line is constant. This value is obtained from the comparison among the theoretical background (in section 2.6) and the reference study [2]. Figure 4.3 and 4.4 present V^*, the ratio of mean velocity and maximum velocity, along flow direction at each point of the duct versus L^*, the normalized term, of the entrance length (L_e) and the hydraulic diameter of the duct (D_h) for laminar and turbulent flow, respectively. To ensure that the velocity lines are constant, the derivative term ($V^{*'}$) of V^* with respect to L^* is plotted.

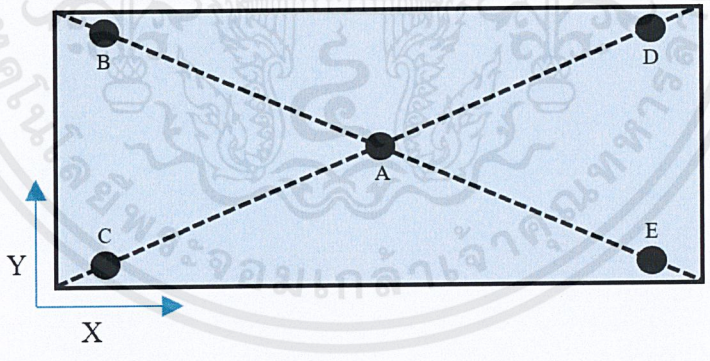

Figure 4.2 Position of the collected velocity data for x-y plane

The characteristic lines of a blank case gradually change from the inlet to the outlet of the duct because there is no obstacle. When the damper is installed in the duct. Each type of the damper (parallel and opposed with different in blade alignment) is fixed its inclination at 45-degree angle. In turbulent flow, their characteristic lines (see Figure 4.9, 4.10, 4.11 and 4.12), indicate that the flow can be disturbed by damper's blades easier than the laminar flow (see Figure 4.5, 4.6, 4.7 and 4.8).

When the flow characteristic (laminar flow and turbulent flow) is fixed: turbulent flow, while the damper's type is opposed-blades. The simulation results are shown in Figure 4.11 and 4.12, indicate that the flow can be disturbed by damper's blades easier than parallel-blades (see Figure 4.9 and 4.10) due to the mean velocity over the length of the duct for damper's blades style-IV case is the most fluctuated. Summary of the results are shown in Table 4.2.

4.2.1 Effect of flow characteristic

Figure 4.3 and 4.4 illustrate the predictions of the mean velocity distribution along flow direction in a blank duct with two different flow characteristics (laminar and turbulent flow). The trend of all characteristic lines gradually change from the inlet to the outlet of the duct. The further details as Table 4.3 and 4.4 present the cross-sectional contour of z-velocity for various Z/D of laminar and turbulent flow respectively. It is found that the developing of the core flow in laminar flow is less than turbulent flow at the same Z/D. In a laminar boundary layer, any exchange of mass or momentum takes place only between adjacent layers. A turbulent boundary is marked on the other hand by mixing across several layers of it, the mixing of fluid may be seen moving across. Thus, there is an exchange of momentum on a much bigger scale compared to a laminar boundary layer (see Figure A.1 and A.2). So, the turbulent flow is requiring distance to fully developed flow less than the laminar flow.

4.2.2 Effect of damper's type

Figure 4.5 to 4.12 illustrate the prediction of the mean velocity distributions along flow direction of various damper's type with fixed 45-degree angle. When flow characteristic is fixed, the opposed-blades damper is induced to entrainment phenomena at the downstream direction as a free plane jet flow (see Figure 4.17, 4.18, 4.21 and 4.22). The entrainment is the fluid transportation across an interface between bodies of fluid by a shear induced turbulent flux. Thus, the momentum transfer of opposed-blades dampers is easily than parallel-blade dampers. The parallel-blade dampers occur wake at the downstream direction (see Figure 4.15, 4.16, 4.19 and 4.20). Therefore, the momentum transfer between layer is less than another type. So, the opposed-blade dampers are requiring the entrance length less than parallel blades dampers.

4.2.3 Effect of blade alignment

Unless the damper's type, blade alignment is also affect to the entrance length. Figure 4.9 and 4.10 illustrate the prediction of the mean velocity distributions along flow direction of the parallel-blade damper but different in blade alignment (style-I and II). The results of both style are similar (see Figure 4.19 and 4.20). Figure 4.11 and 4.12 illustrate the prediction of the mean velocity distributions along flow direction of the both opposed-blade damper's styles (style-III and IV), respectively. It is found that the both of opposed-blade dampers is induced to plane jet flow at the downstream direction and plane wall jet flow at the near wall region, then mass of fluid is entrained in all direction and increase the momentum transfer. For the opposed-blade damper style-III, the wall bounded effect at the core flow is induced the entrain mass of fluid less than other style. So, the opposed-blade damper style-IV requires the shortest entrance length (see Figure 4.21 and 4.22).

By the way, the additional information of the total pressure value, that is predicted for each geometry, also is available here. Figure 4.23 illustrates the pressure distribution in the blank rectangular duct. It is found that the pressure value continually drops over the length of the duct (from the inlet) due to the friction loss at the wall. Figure 4.24, 4.25, 4.26 and 4.27 illustrate the pressure distribution in the region nearby the damper for style-I, II, III and IV respectively. It is found that there is a pressure difference between the high pressure on the downstream surface of the flat plate in the near wake thus causing a pressure drag force on the flat plate in the direction of air flow. Consequently, this behavior also let the loss of momentum at the flat plate beyond at the wall only as the air flow in the blank duct. Such pressure difference is the largest in case of style-III thus the largest size of the reversed flow region occurs behind the flat plate while a pressure difference in style-I, II and IV becomes smaller as compared to the style-III (see Figure A.3 to A.10).

Table 4.2 The simulation results of entrance length

L_e/D	Blank duct	I	II	III	IV
Laminar flow (Re = 1,000)	64	60	57	55	46
Turbulent flow (Re = 4,000)	25	22	21	20	17

Table 4.3 The cross-sectional contour of z-velocity for various Z/D of laminar flow

	Z/D	Laminar flow
7.41 6.67 5.56 4.45 3.33 2.22 1.48 0 ($x10^{-2}$ m/s)	13	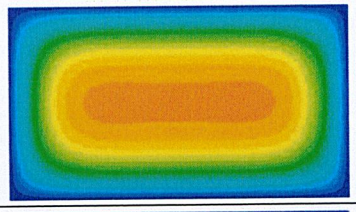
	18	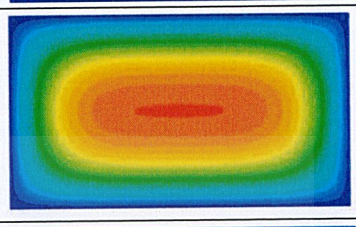
	22	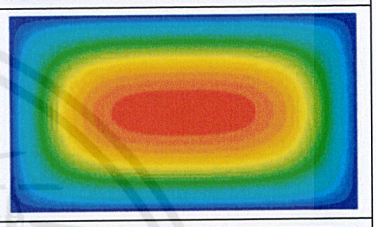
	50	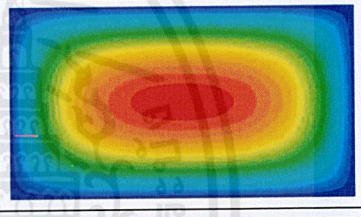
	65	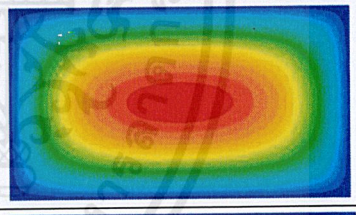
	88	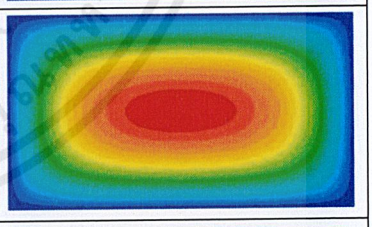
	100	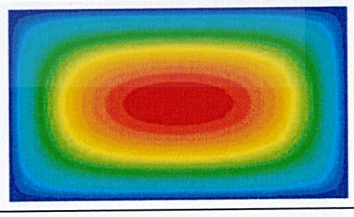

Table 4.4 The cross-sectional contour of z-velocity for various Z/D of turbulent flow

	Z/D	Turbulent flow
1.90 1.71 1.43 1.05 0.66 0.55 0.38 0 (m/s)	13	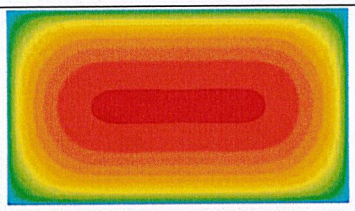
	18	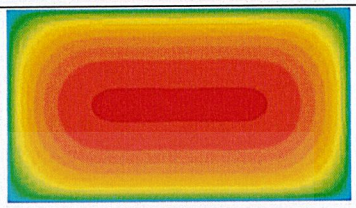
	22	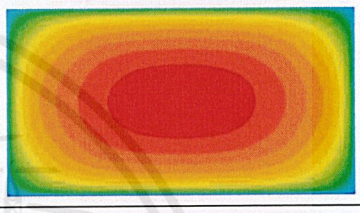
	50	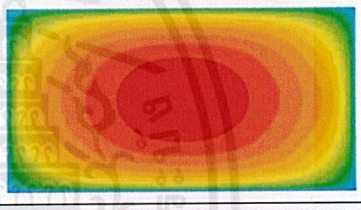
	65	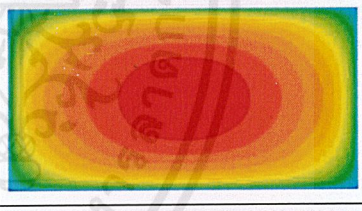
	88	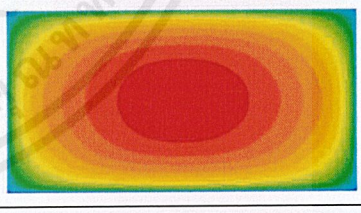
	100	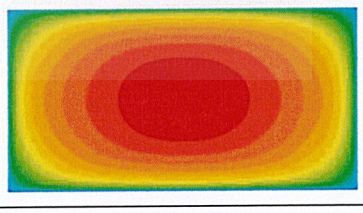

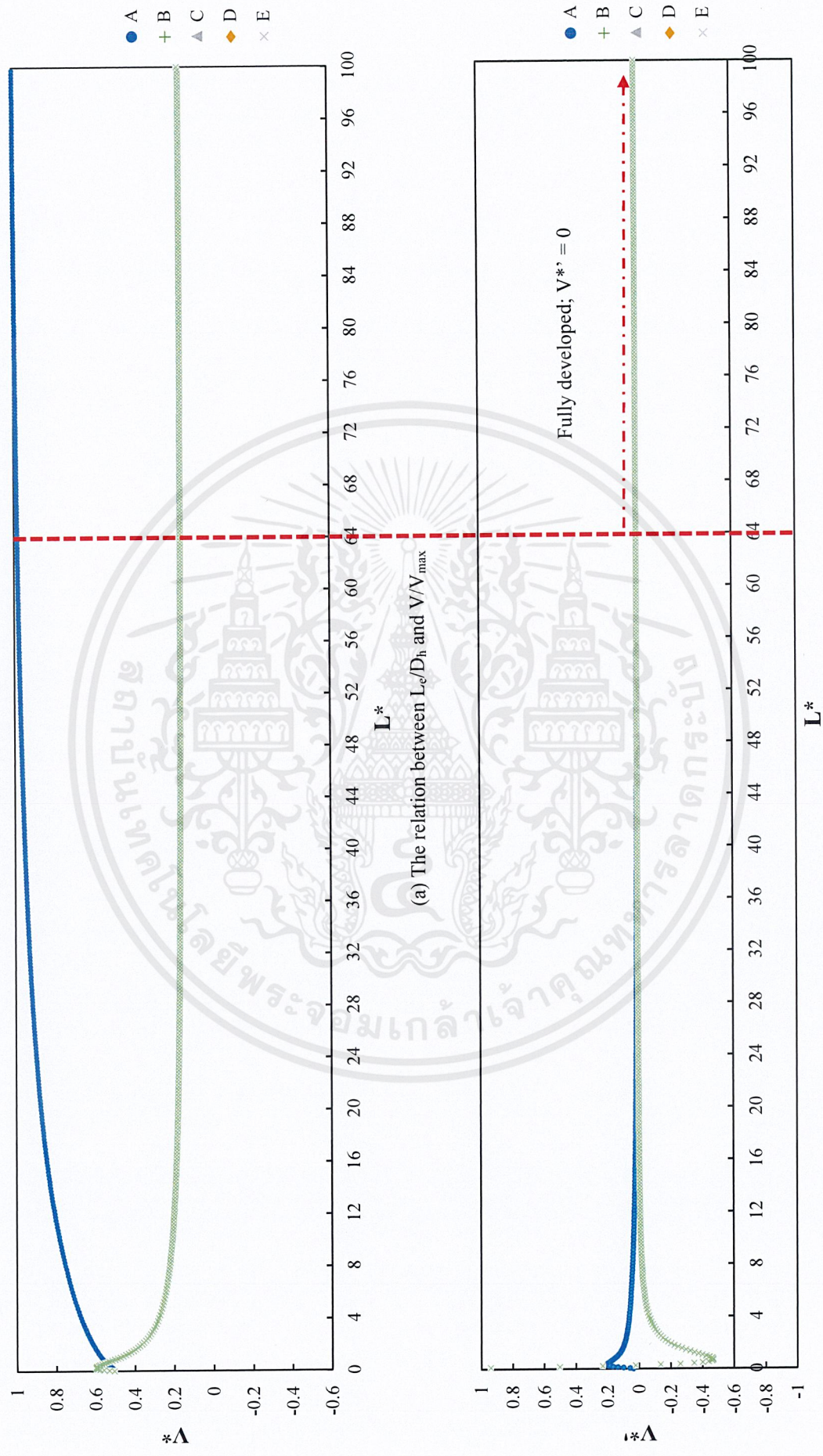

Figure 4.3 Simulation results of laminar flow in blank rectangular duct

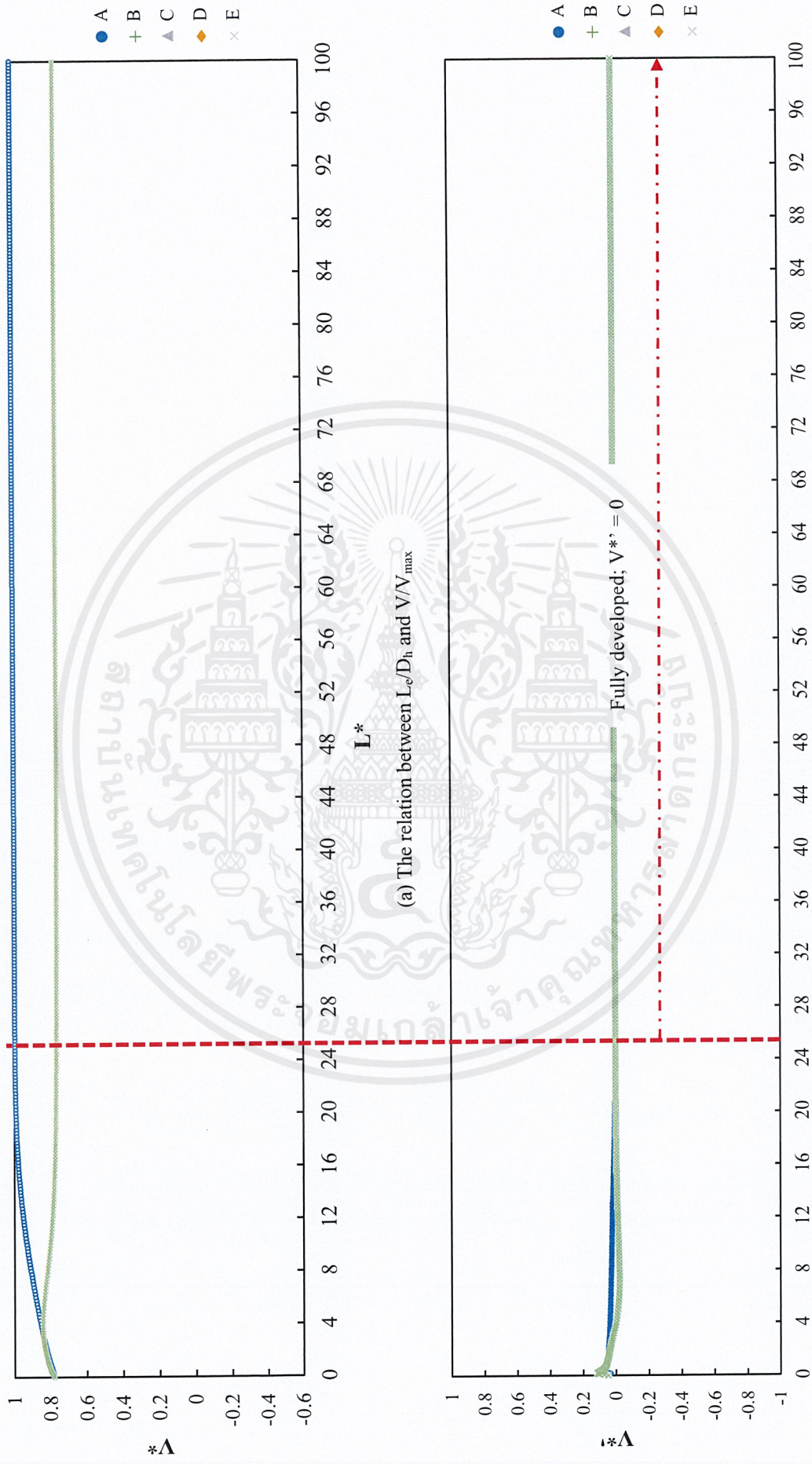

Figure 4.4 Simulation results of turbulent flow in blank rectangular duct

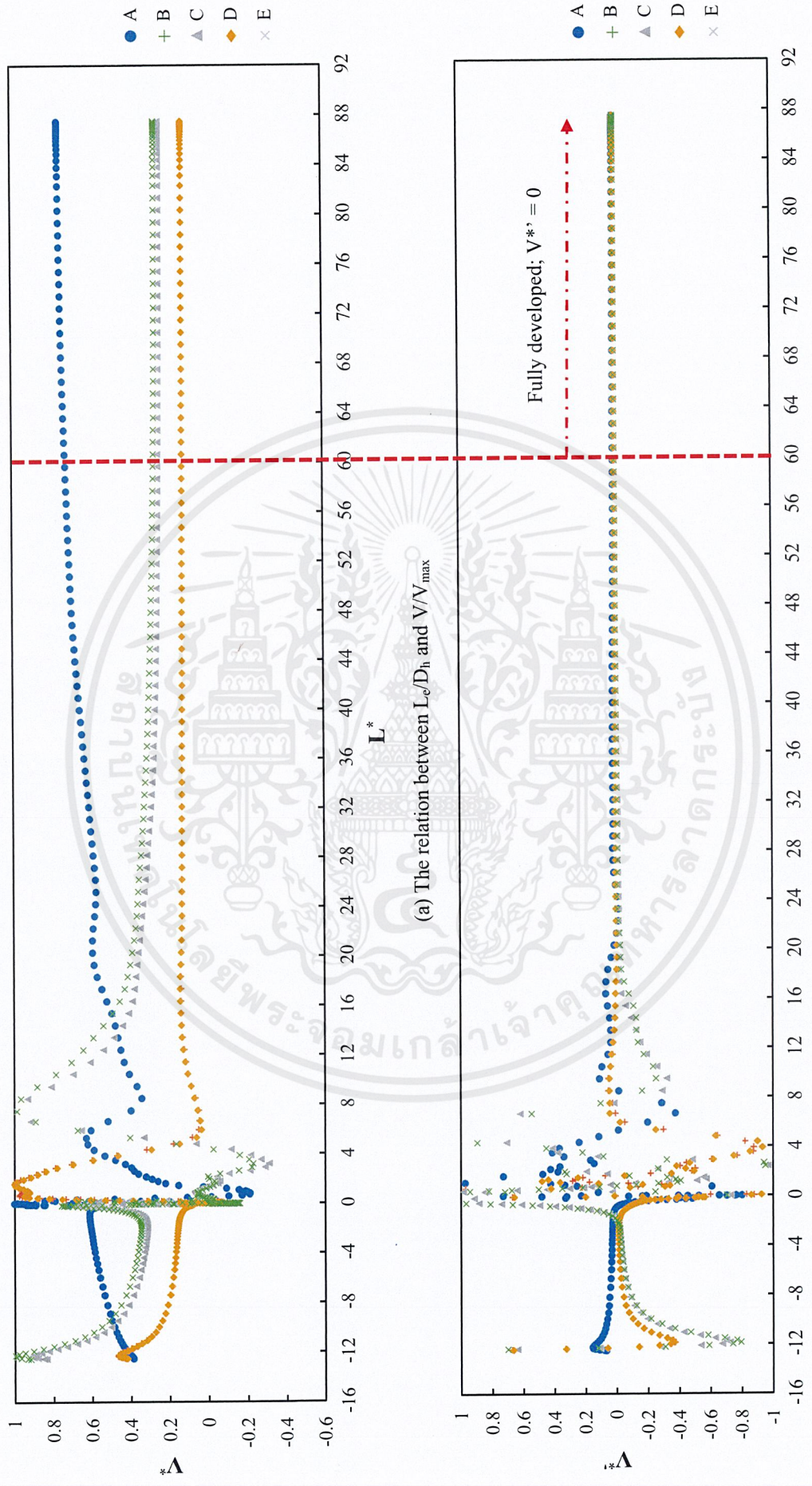

(b) The relation between L_e/D_h and derivative of z-velocity

Figure 4.5 Simulation results of damper style-I in laminar region

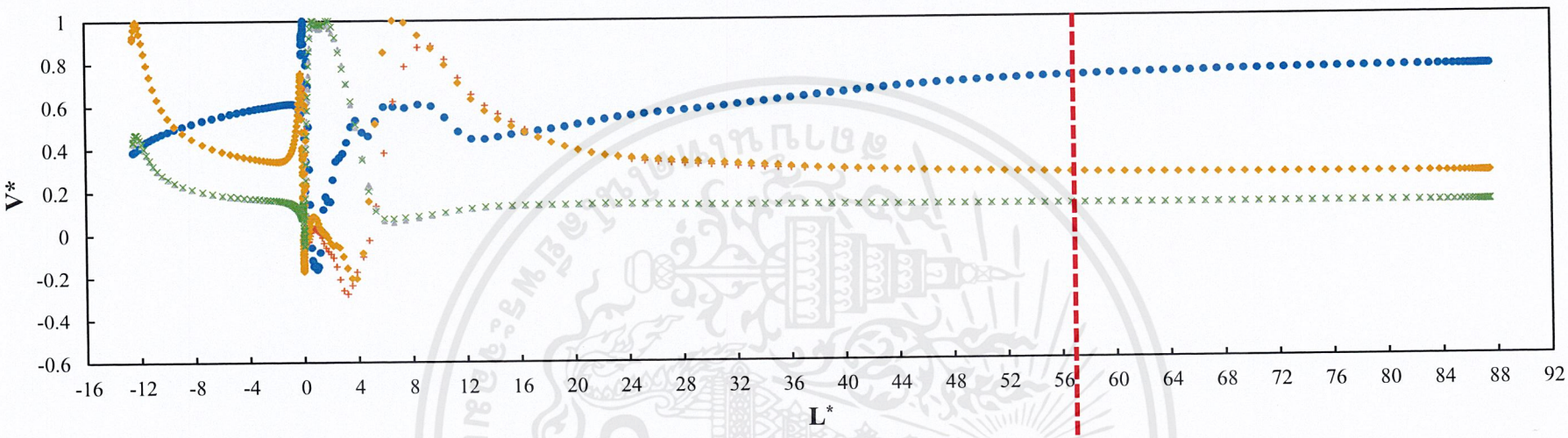

(a) The relation between L_e/D_h and V/V_{max}

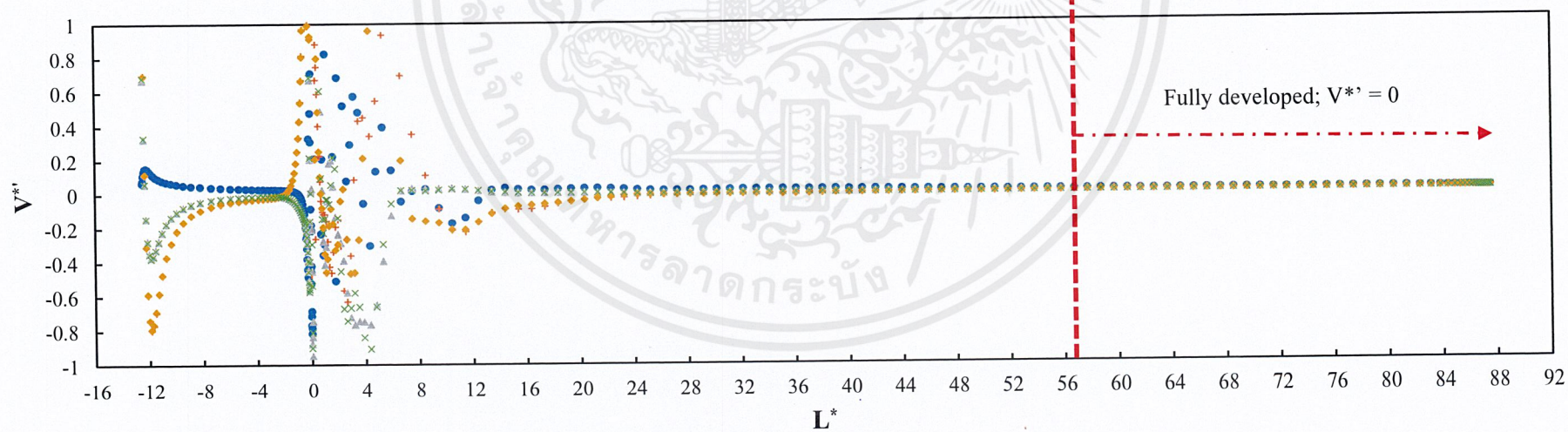

(b) The relation between L_e/D_h and derivative of z-velocity

Figure 4.6 Simulation results of damper style-II in laminar region

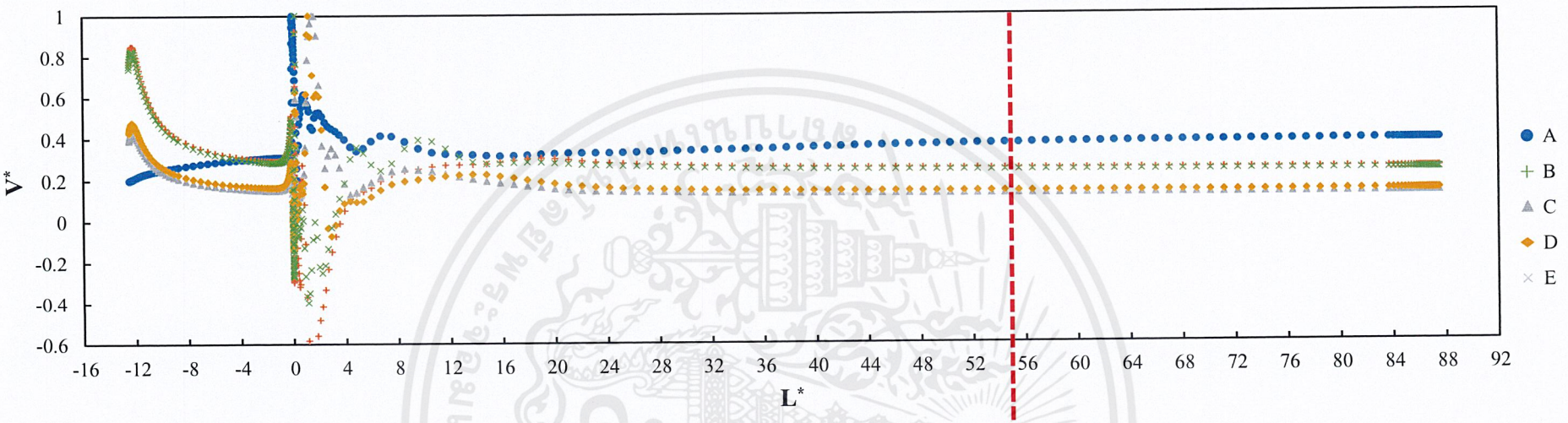

(a) The relation between L_e/D_h and V/V_{max}

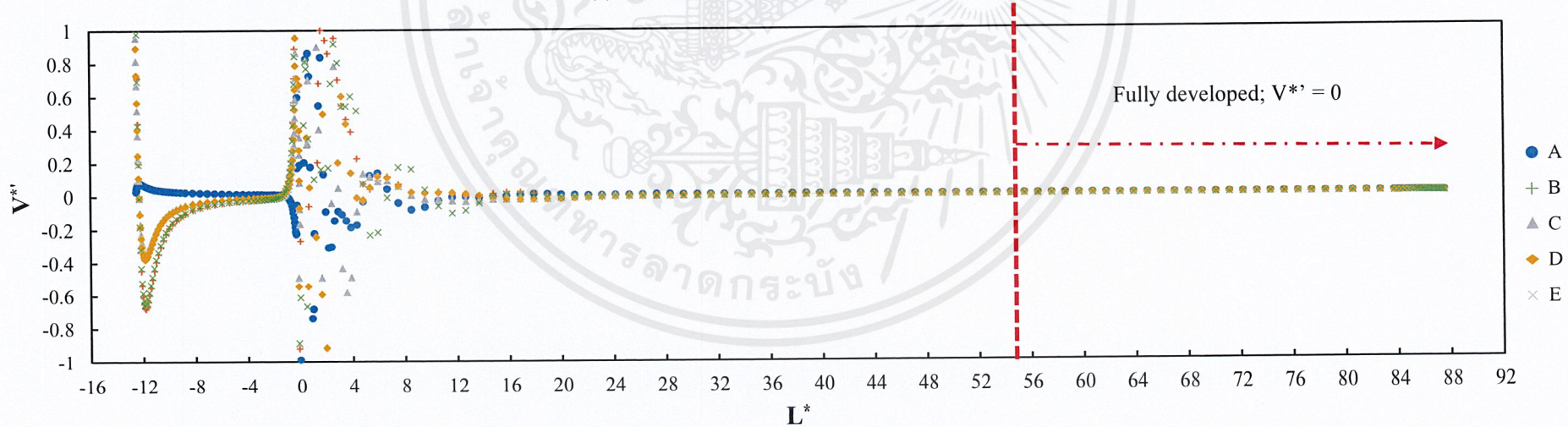

(b) The relation between L_e/D_h and derivative of z-velocity

Figure 4.7 Simulation results of damper style-III in laminar region

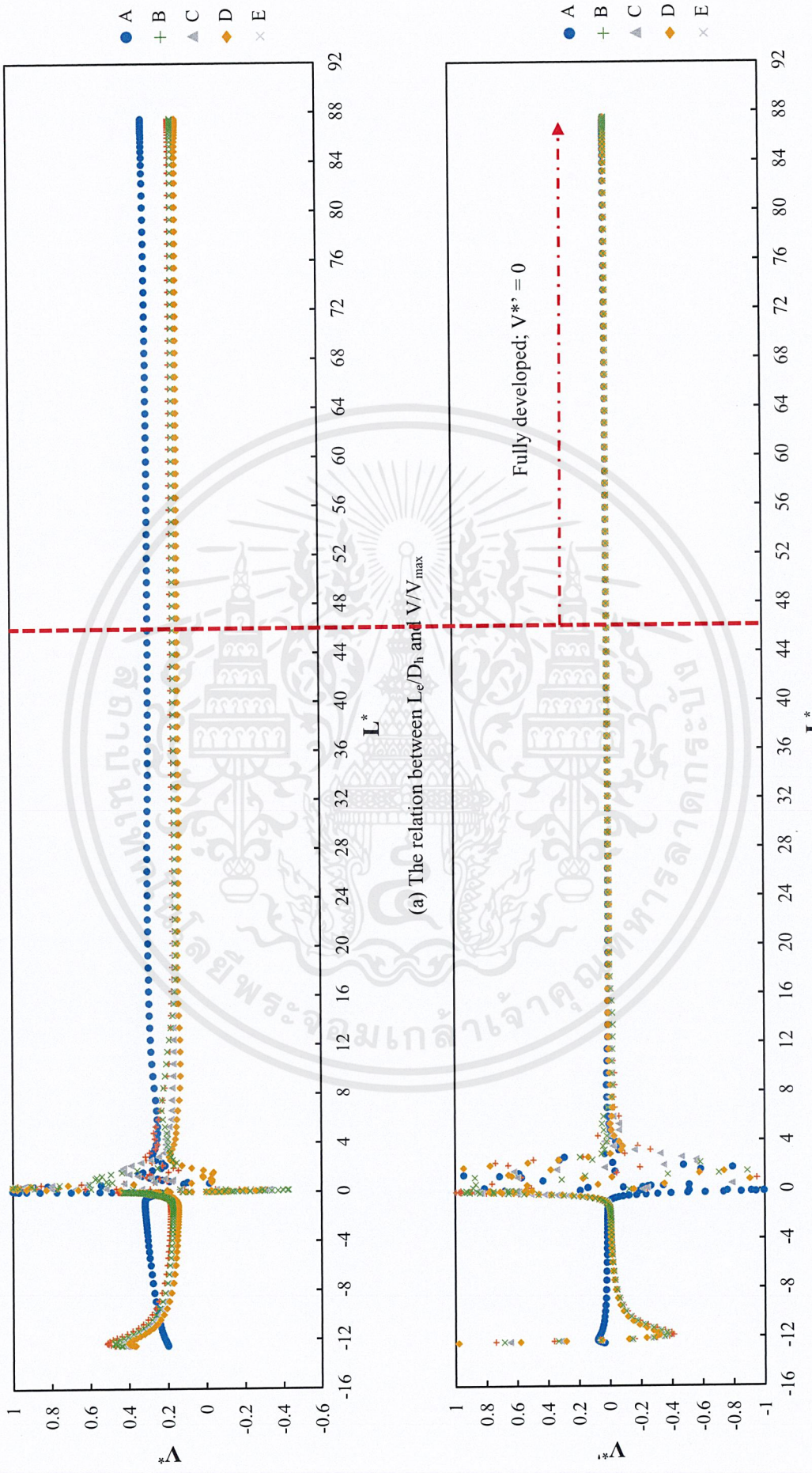

Figure 4.8 Simulation results of damper style-IV in laminar region

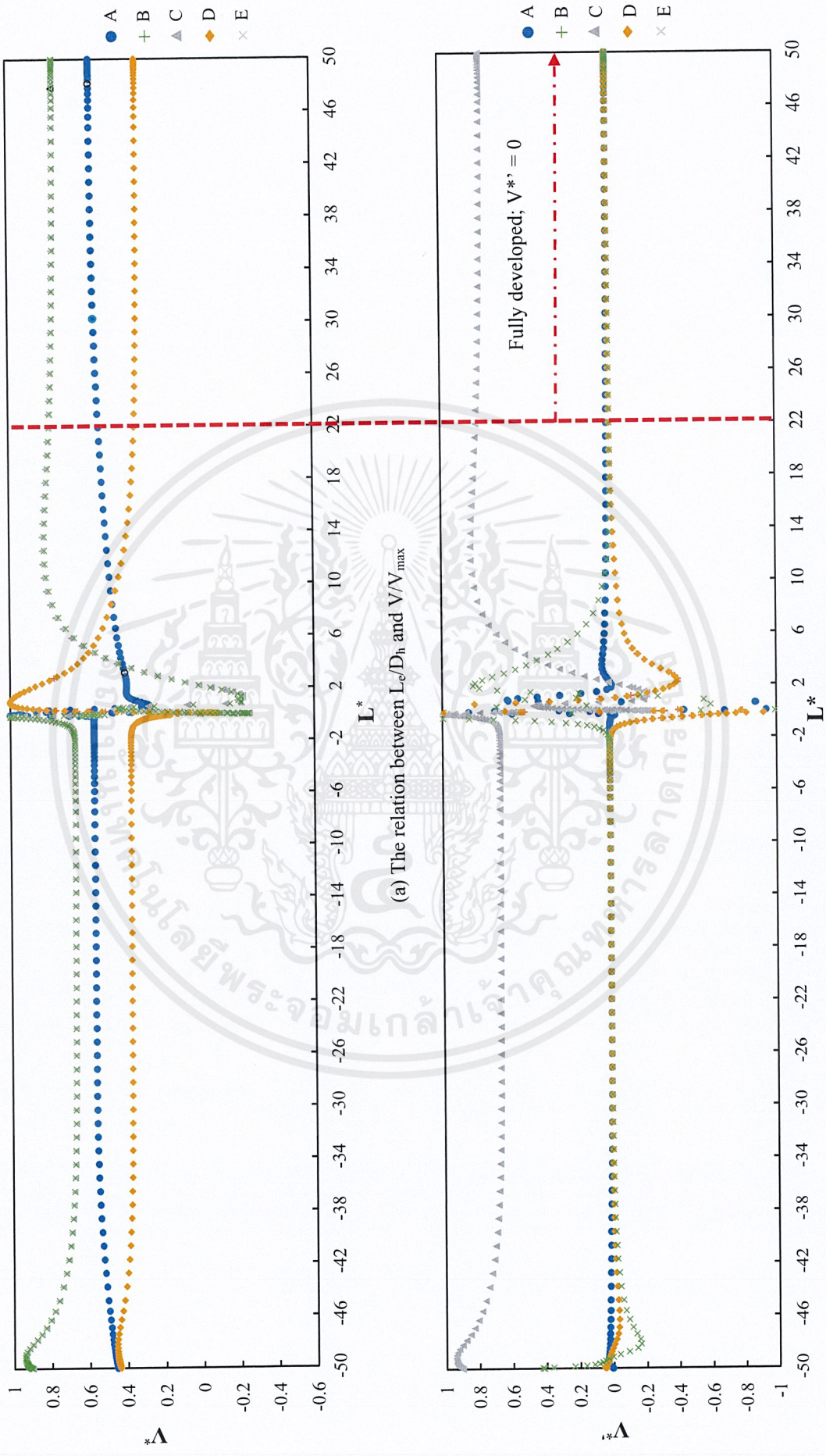

Figure 4.9 Simulation results of damper style-I in turbulent region

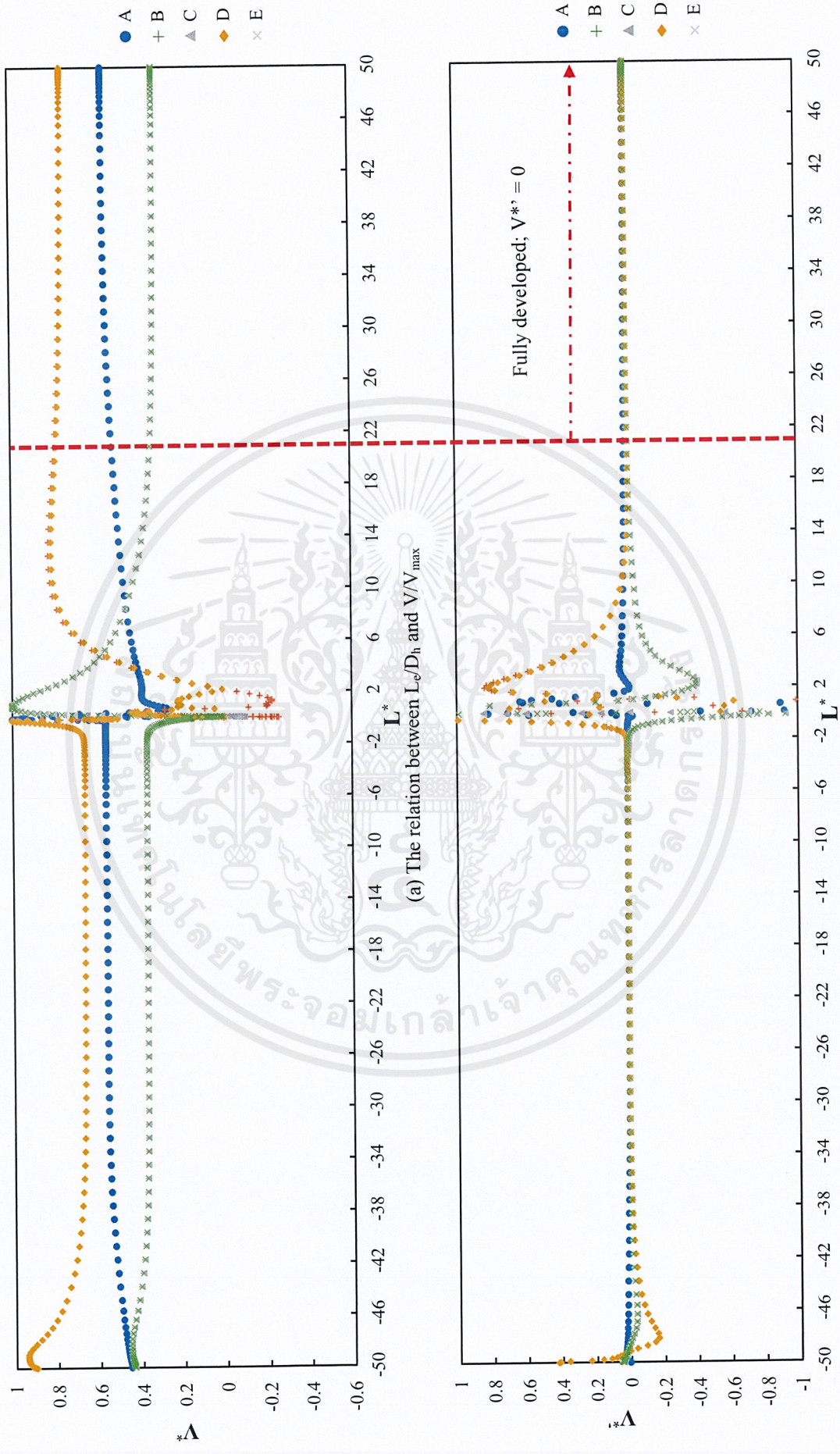

Figure 4.10 Simulation results of damper style-II in turbulent region

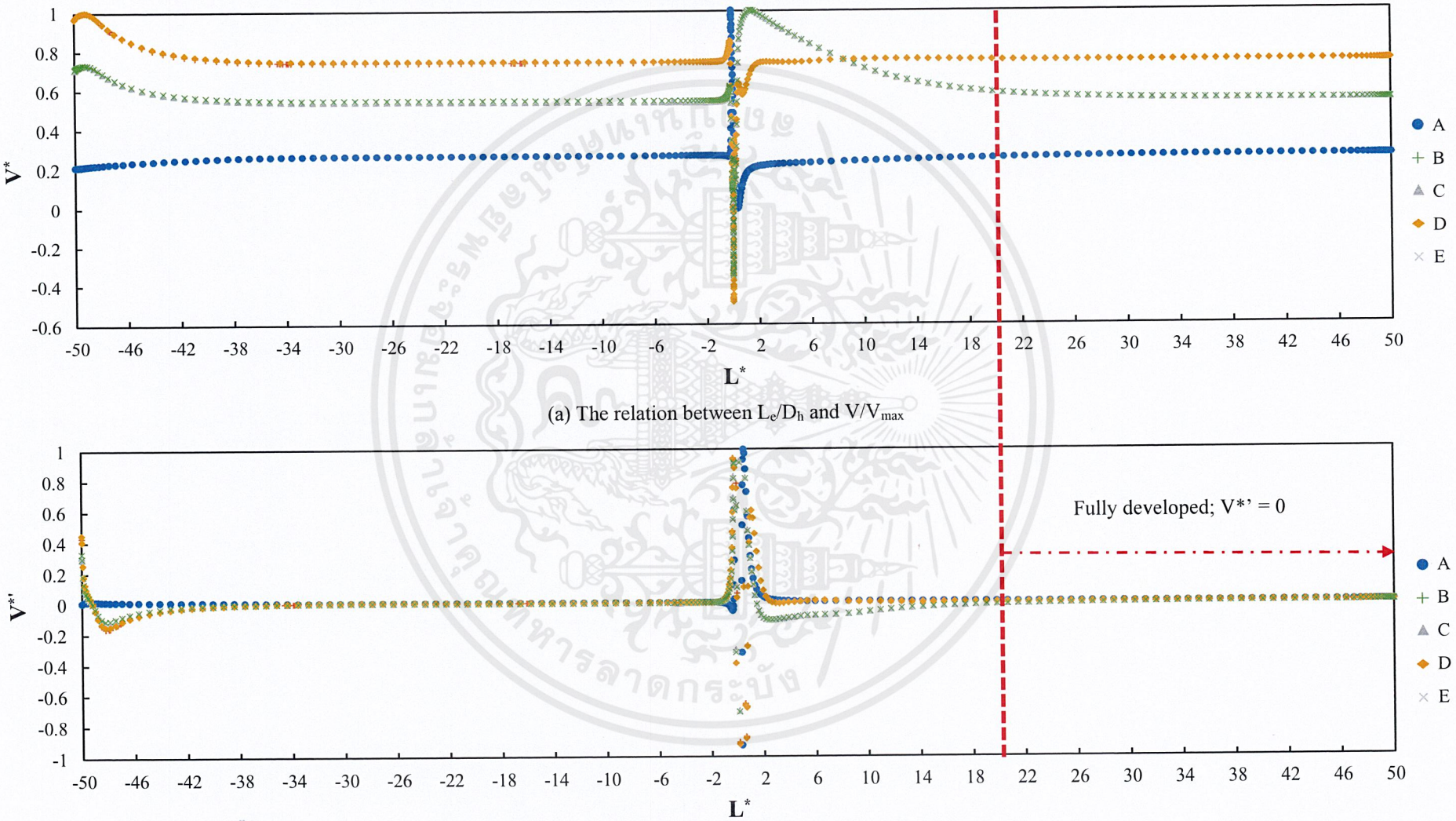

(b) The relation between L_e/D_h and derivative of z-velocity

Figure 4.11 Simulation results of damper style-III in turbulent region

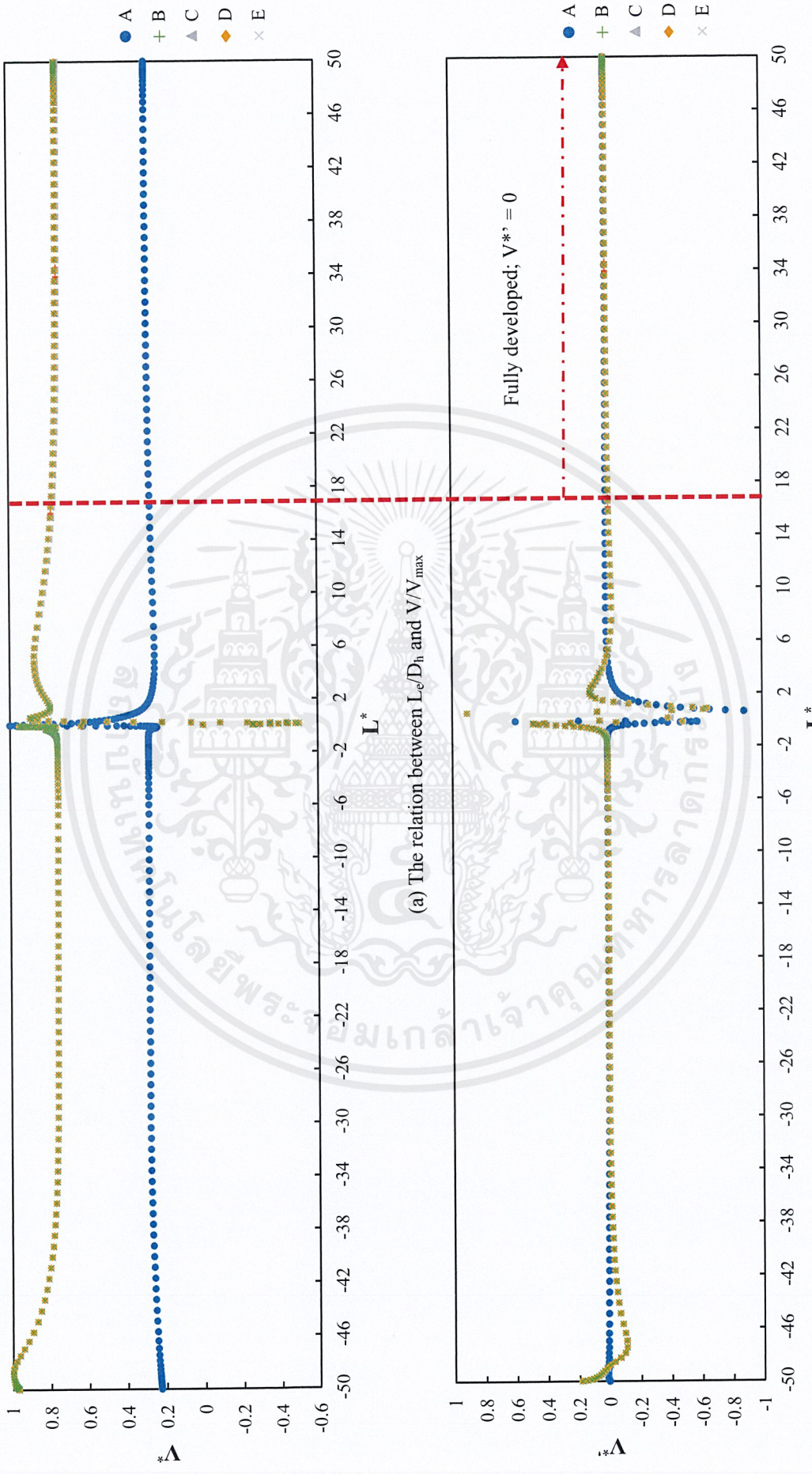

Figure 4.12 Simulation results of damper style-IV in turbulent region

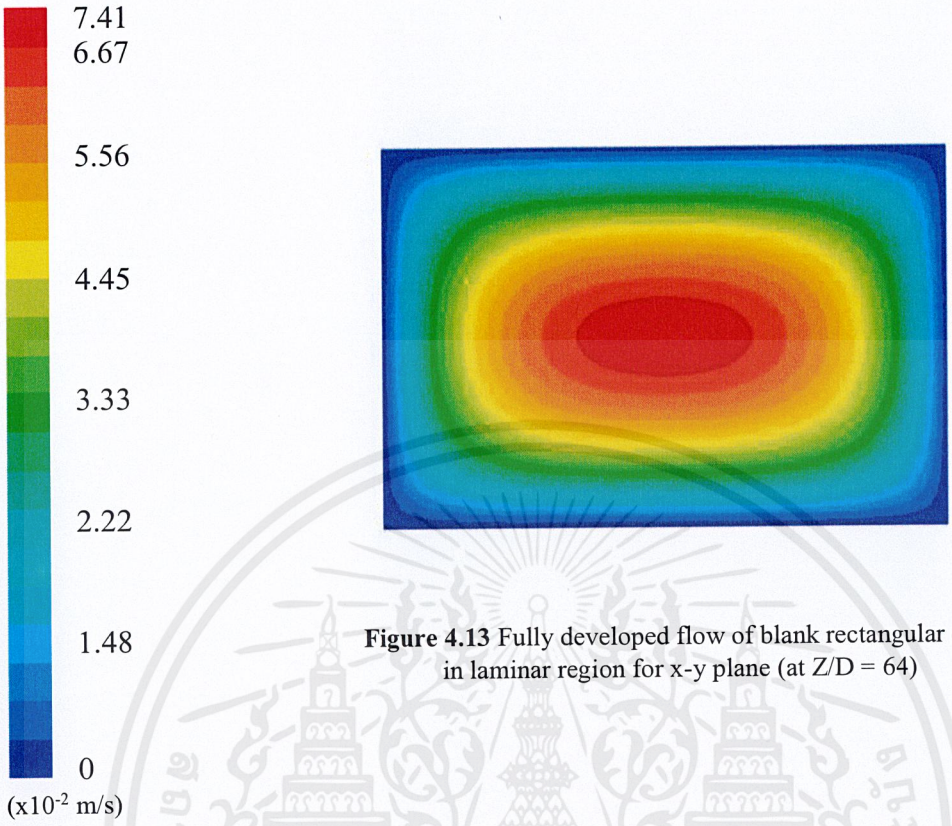

Figure 4.13 Fully developed flow of blank rectangular duct in laminar region for x-y plane (at Z/D = 64)

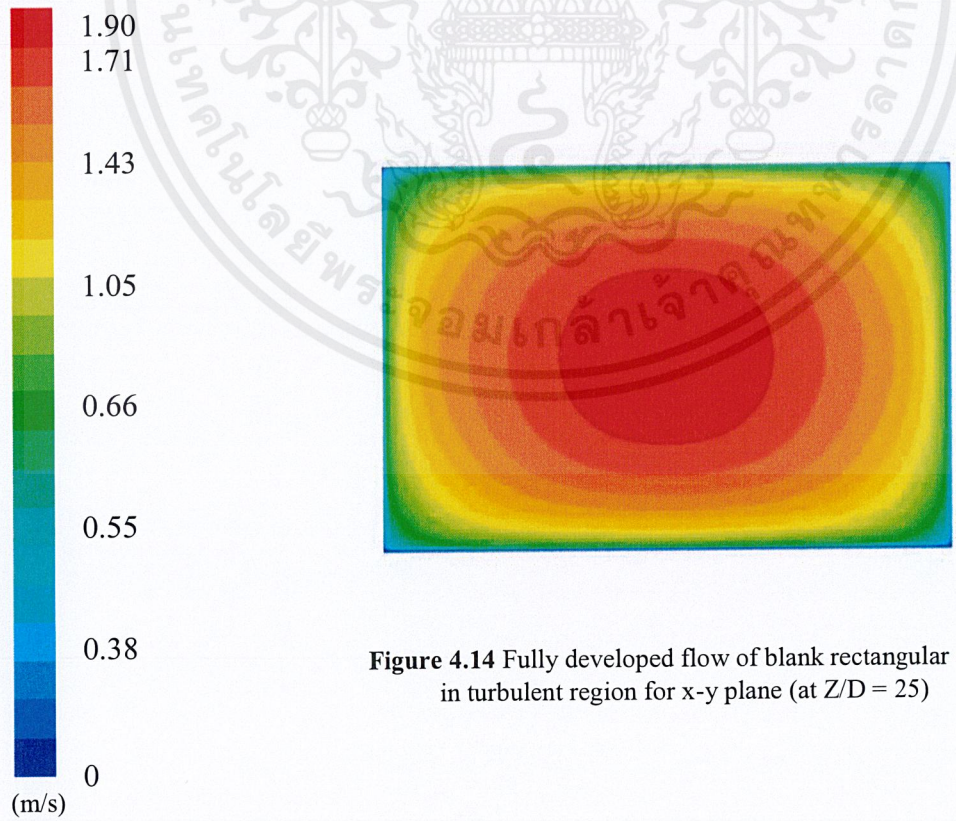

Figure 4.14 Fully developed flow of blank rectangular duct in turbulent region for x-y plane (at Z/D = 25)

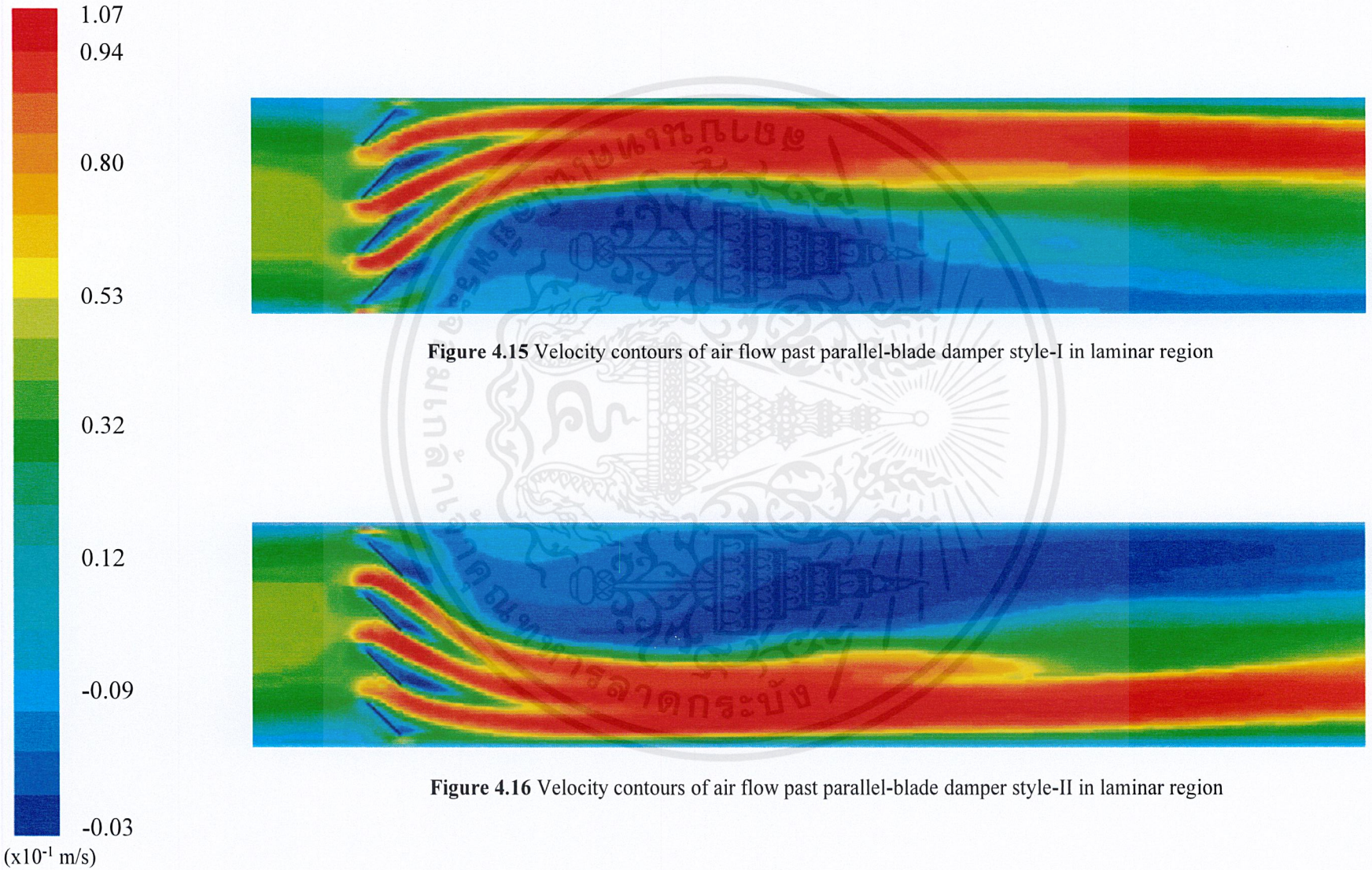

Figure 4.15 Velocity contours of air flow past parallel-blade damper style-I in laminar region

Figure 4.16 Velocity contours of air flow past parallel-blade damper style-II in laminar region

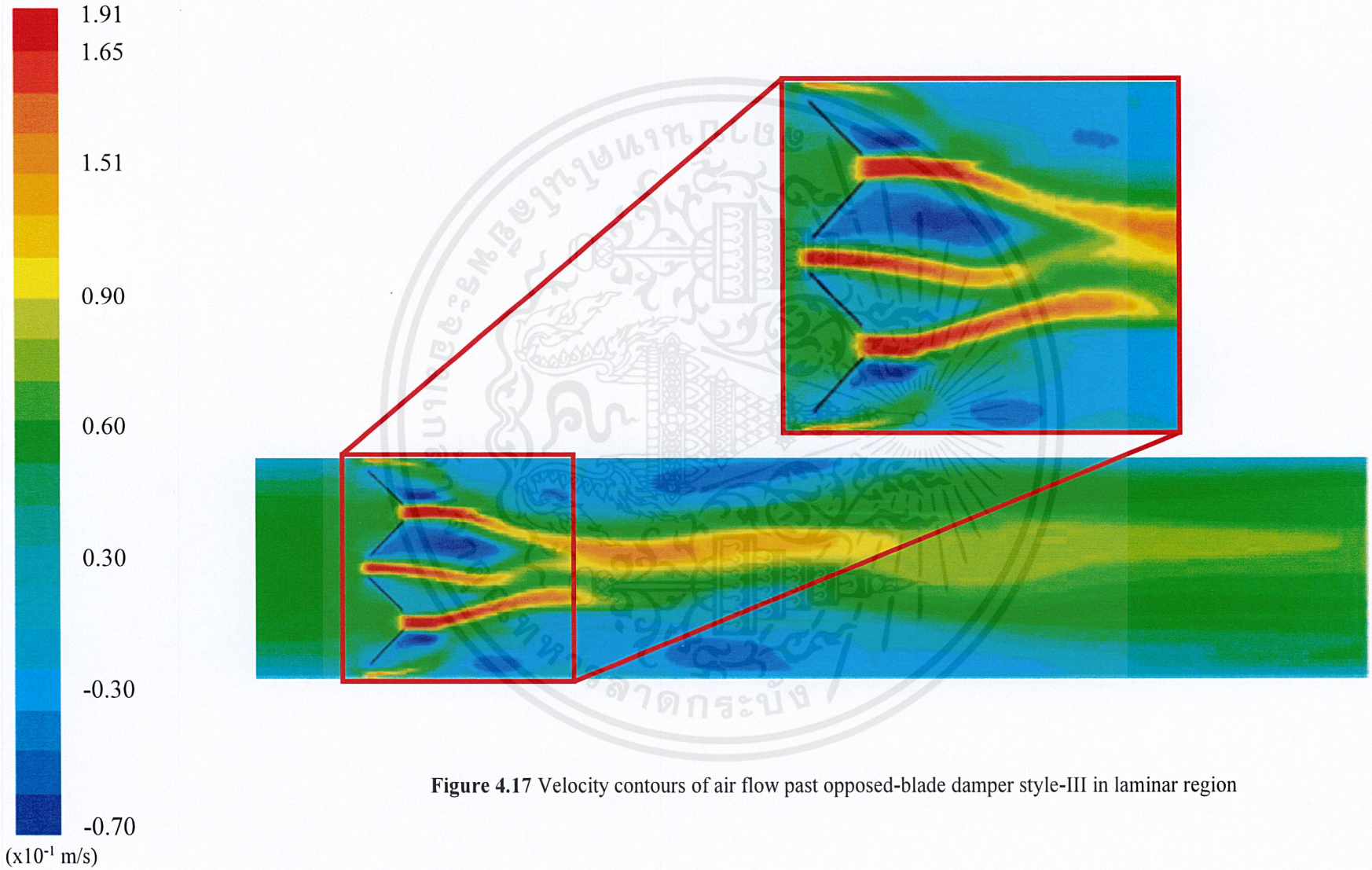

Figure 4.17 Velocity contours of air flow past opposed-blade damper style-III in laminar region

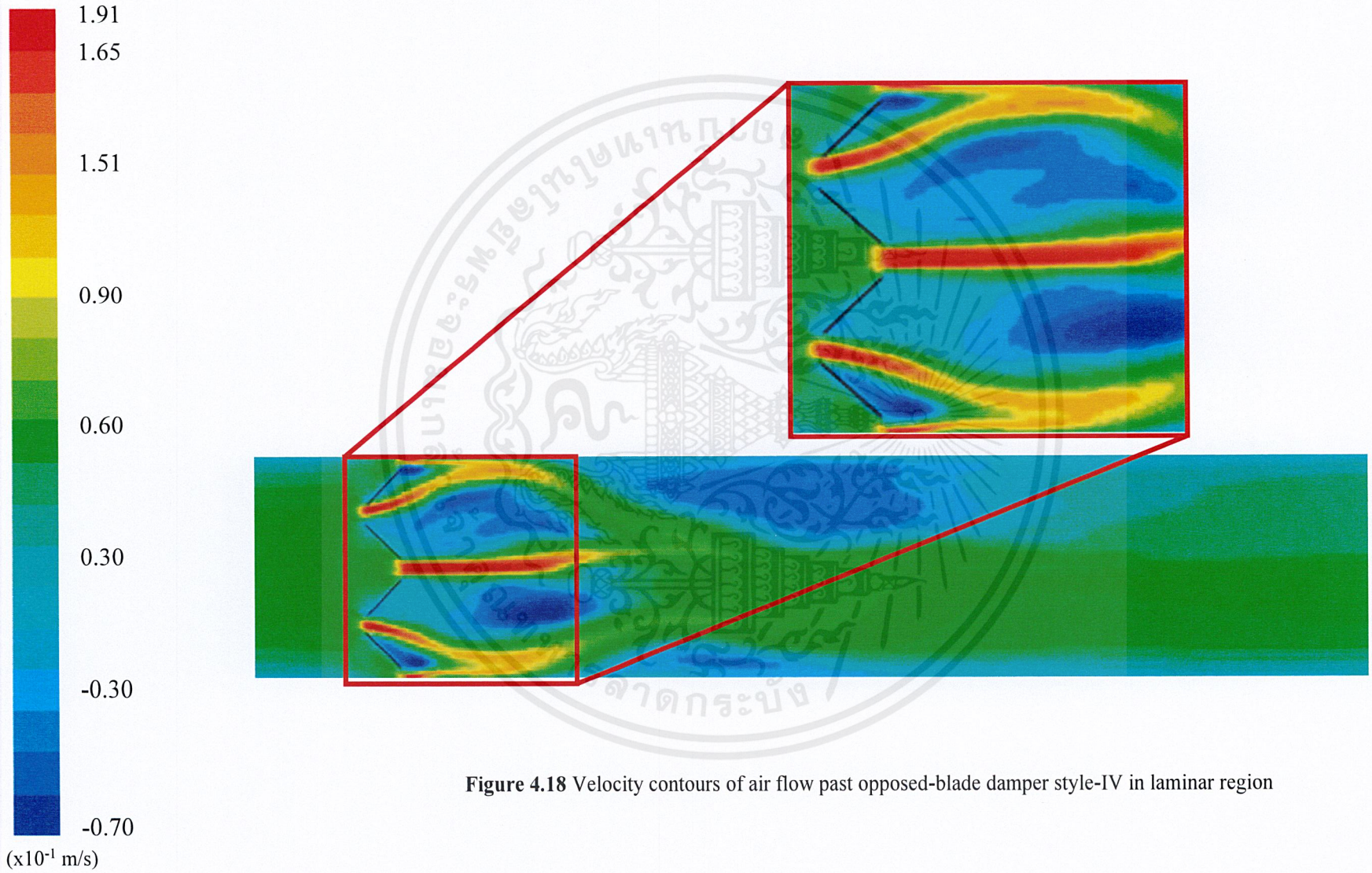

Figure 4.18 Velocity contours of air flow past opposed-blade damper style-IV in laminar region

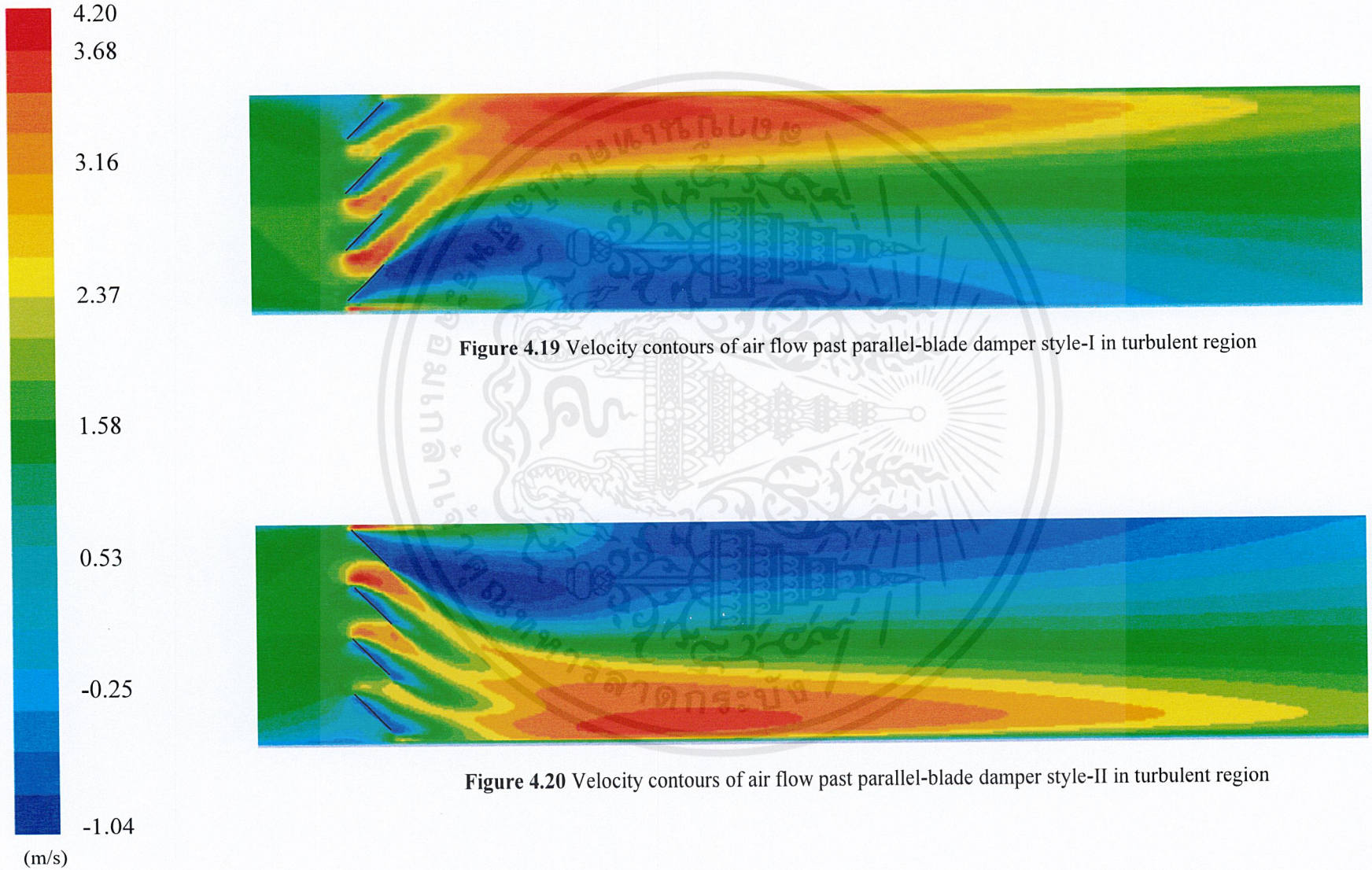

Figure 4.19 Velocity contours of air flow past parallel-blade damper style-I in turbulent region

Figure 4.20 Velocity contours of air flow past parallel-blade damper style-II in turbulent region

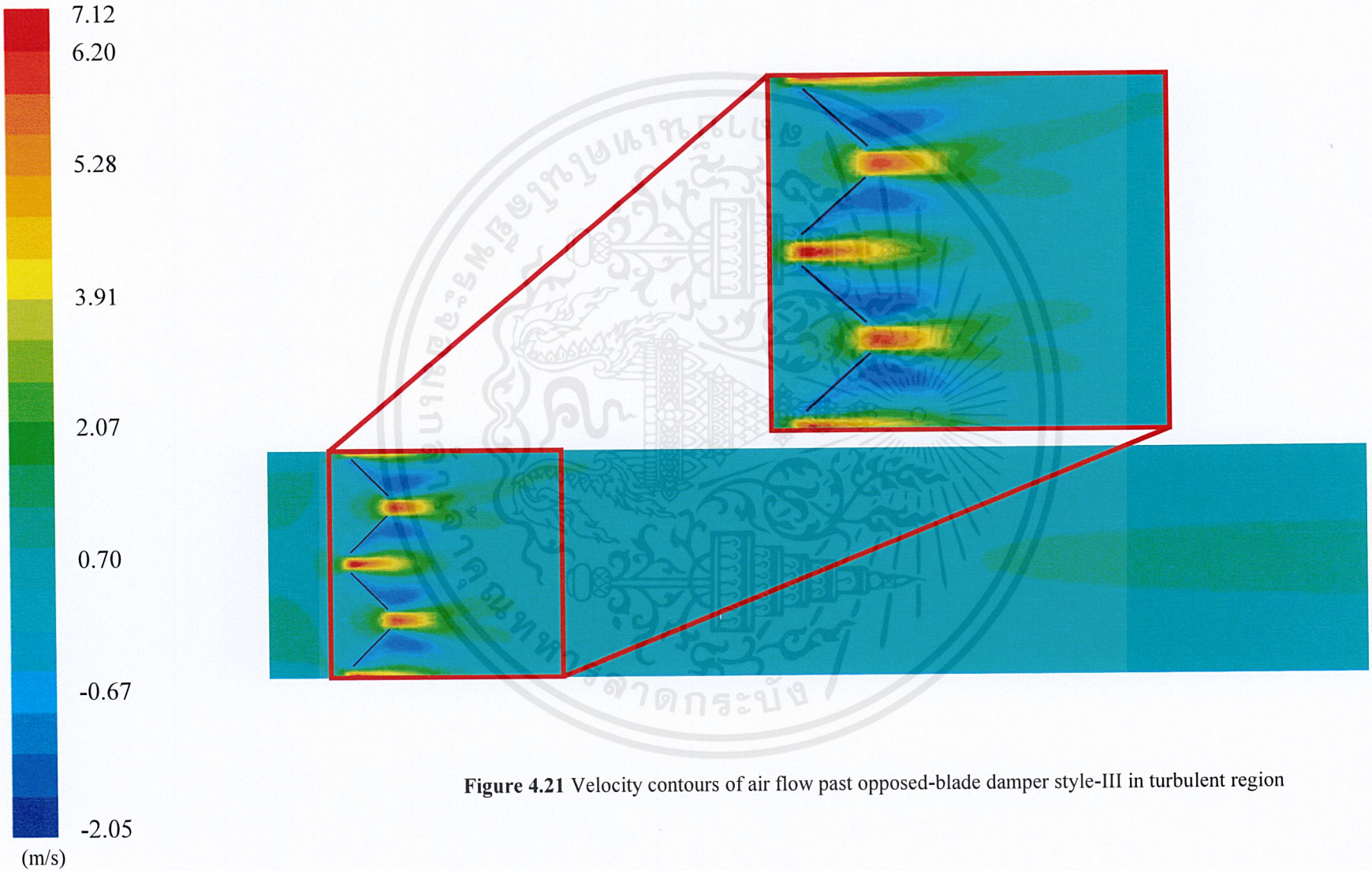

Figure 4.21 Velocity contours of air flow past opposed-blade damper style-III in turbulent region

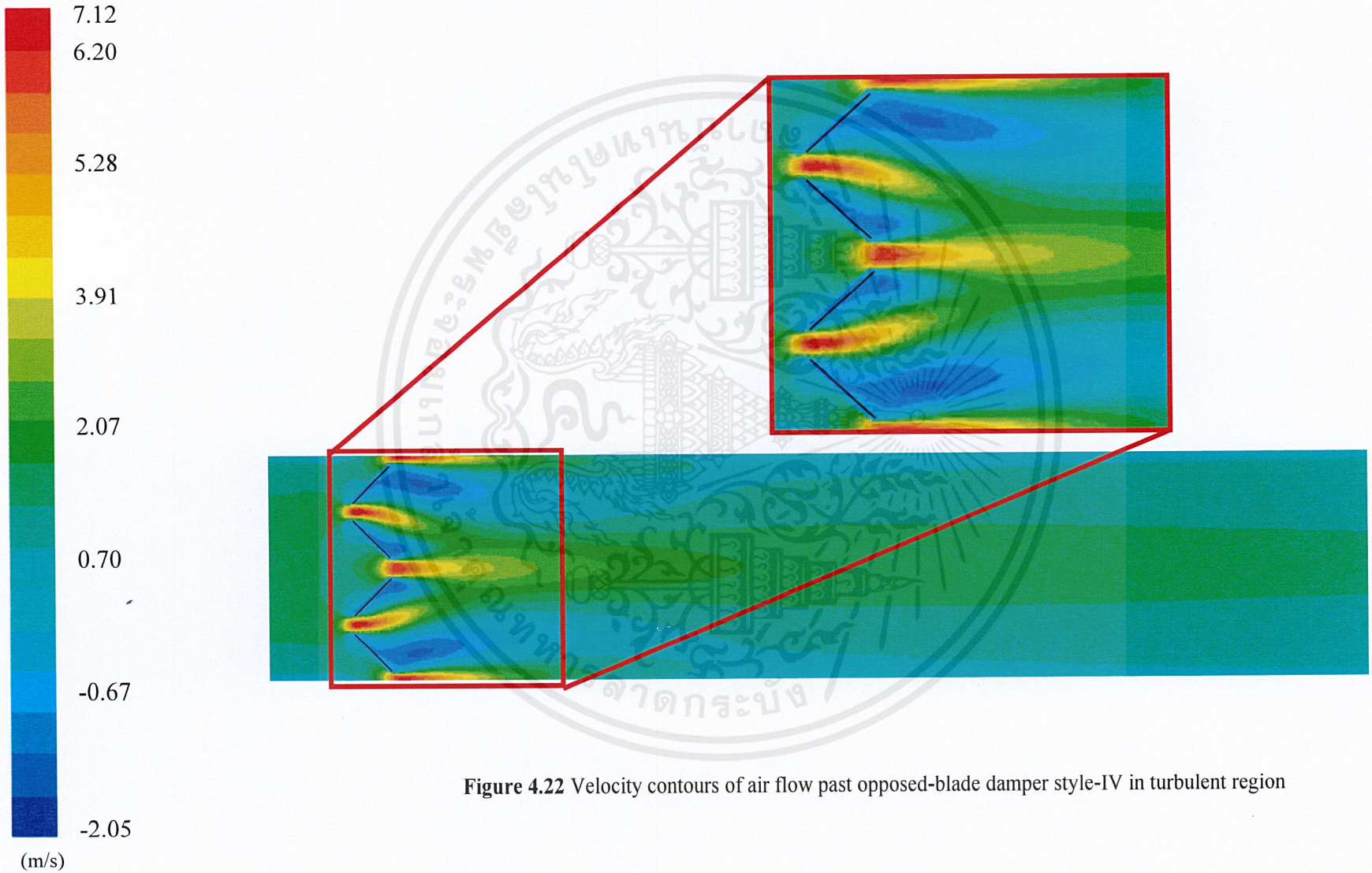

Figure 4.22 Velocity contours of air flow past opposed-blade damper style-IV in turbulent region

Figure 4.23 Pressure contours in a blank rectangular duct of turbulent flow

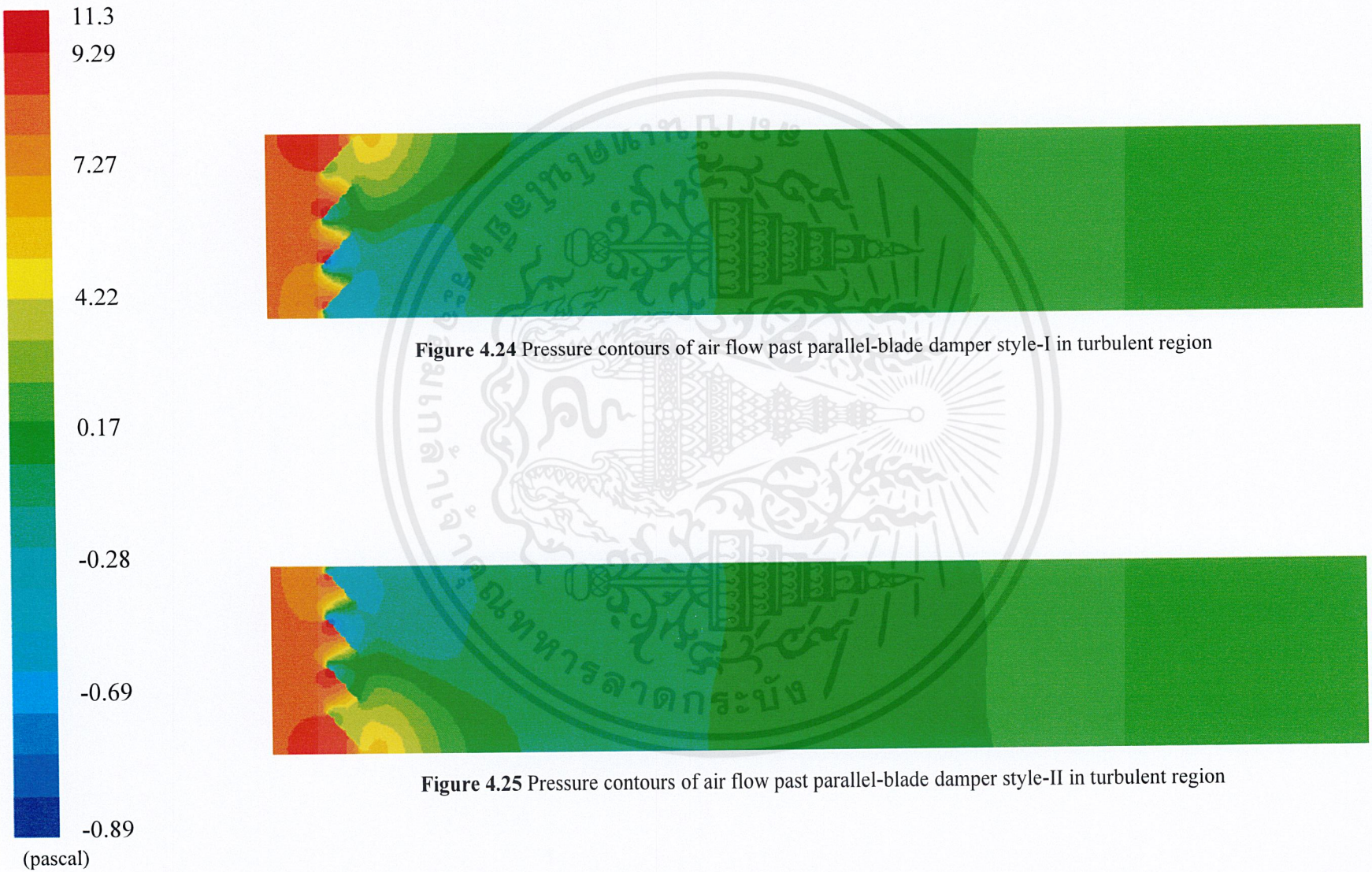

Figure 4.24 Pressure contours of air flow past parallel-blade damper style-I in turbulent region

Figure 4.25 Pressure contours of air flow past parallel-blade damper style-II in turbulent region

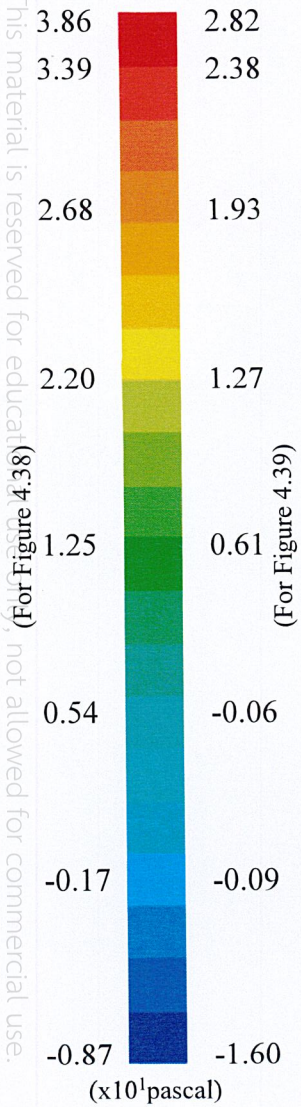

Figure 4.26 Pressure contours of air flow past opposed-blade damper style-III in turbulent region

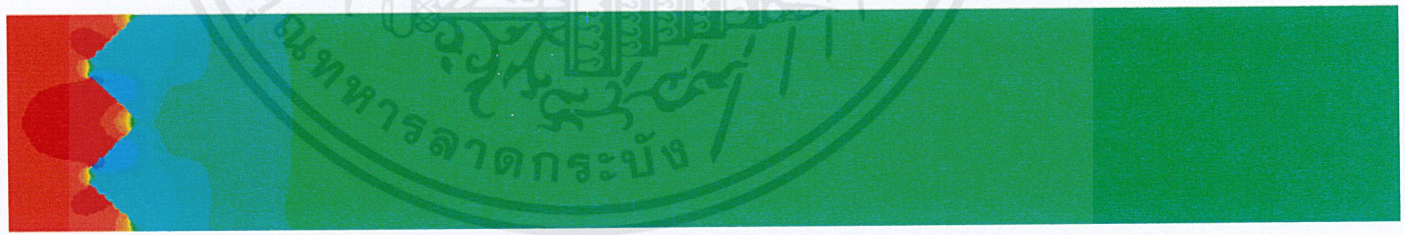

Figure 4.27 Pressure contours of air flow past opposed-blade damper style-IV in turbulent region

CHAPTER V
CONCLUSIONS AND RECOMMENDATION

5.1 Conclusions

This project was applied the computational fluid dynamics to predict the phenomena of the air flow past the opposed and parallel inclined flat plates in a rectangular duct. The simulation model is validated with the study of Wattananusorn [2], correlation of Re function [9] and experimental result [12]. The ANSYS FLUENT 14.5 finite volume CFD code was adopted to solve steady state three-dimensional flow inside the duct. The Reynolds averaged equations with standard k-ε turbulence model were used to simulate the mean flow properties and turbulence. The simulation results of validation shown that the grid numbers 1,379,096 cells are accurate to simulate the flow inside the duct and also consume the calculation time to simulate properly.

According to the simulation results, it can be distinguished for three influences that affect to the entrance length as bellows:

(1) Flow characteristic

(2) The type of damper

(3) Blade alignment

In case of flow characteristic of the air flow, according to subsection 4.2.1. It is remarked that at the same type of the damper and same blade alignment, the air flow with higher Re as 4,000 (Turbulent flow) requires the distance for fully developed flow less than the lower Re as 1,000 (Laminar flow) because the momentum can be transferred in radial direction by velocity fluctuations and vigorous mixing. So, the entrance length of turbulent flow is shorter than laminar flow.

Regarding the type of damper, the various types have got different results. According to subsection 4.2.2, it is remarked that at the same flow characteristic, the opposed-blade damper requires the entrance length to be less than the parallel-blade damper because an entrainment phenomenon at the downstream direction. Since entrainments of fluid in both cases generate momentum transfer, leading to fully developed flow occurs easily.

In case of blades alignment, its characteristic of this research are two styles in each damper's types. According to subsection 4.2.3, it is remarked that at the same flow

characteristic and same damper's type. For the parallel-blade damper, the difference of both results (style-I and II) is insignificant, on the other hand, in the opposed-blade damper it shows the difference must be taken into account. The opposed-blade damper style-IV requires the shortest entrance length because the free plane jet flow at the downstream direction. The opposed-blade damper style-III has a free plane jet flow with near wall bounded, then momentum transfer is less than another style.

Consequently, the influence of whether (1), or (2), or (3), or all simultaneously. There are surely affects to the entrance length region in the duct.

5.2 Recommendations

1. The installation effect can be reduced by selection of the appropriate damper. The opposed-blade damper style-IV is recommended for this purpose due to expedite the developing to be fully developed flow, moreover it can be applied for air mixing.
2. This project is study the phenomena of fluid flow in a rectangular duct with standard k- ε turbulent model for reduce calculation time. For more accuracy, RNG k- ε turbulent model can be used as represent.
3. This project is study the phenomena of only air flow, if it can apply for studying in term of others fluid that can be using in industrials, and also tend to bring into real situations.

REFERENCES

1. Croome, D.J., and B.M. Roberts, Airconditioning and Ventilation of Buildings, 2nd ed., Oxford, Pergamon, 1981
2. Wattananusorn S., Simulation of Air Flow Past the Parallel Inclined Flat Plates in a Square Duct, Master thesis in Department of Chemical Engineering, Graduate School, Chulalongkorn University, 1997
3. J. H. Ferzigerand M. Peric, Computational Methods for Fluid Dynamics, Springer, 1996
4. P. Wesseling, Principles of Computational Fluid Dynamics, Springer, 2001
5. Celik, I. B., Introductory Turbulence Modeling, Morgantown: s.n., 1999
6. ANSYS, Inc., ANSYS FLUENT Theory Guide, 2012
7. Fox, R. W., and A. T. McDonald, Introduction to Fluid Mechanics, 4th ed., Singapore: John Wiley & Sons, 1994
8. F. M. White, Fluid Mechanics, McGraw-Hill, 1999
9. B. R. Munson, D. F. Young and T.H. Okiisshi, Fundamentals of Fluid Mechanics, John Wiley and Sons, Inc., 1998
10. Yunus A. Cengel and Afshin J. Ghajar, Heat and Mass Transfer: Fundamentals and Applications, 5th ed, McGraw-Hill,2015
11. Mironer, A., Engineering Fluid Mechanics, New York, McGraw-hill, 1979
12. Gerhart, P. M., R. J. Gross, and J. I. Hochstein, Fundamentals of Fluid Mechanics, 2nd ed, Massachusetts, Addison-Wesley, 1992
13. Rayleigh, Notes on Hydrodynamics, Phil. Mag., series 5, vol.2, p.430, 1876
14. Chen, C. J., and W. S. Cheng, Finite Analytic Numerical Solutions of Incompressible Flow Past Inclined Axisymmetric Bodies, University of Iowa, Iowa Institute of Hydraulic Research Report, 1987
15. Cherdron, W., F. Durst, and J. H. Whitelaw, Asymmetric Flows and Instabilities in Symmetric Ducts with Sudden Expansions, J. Fluid Mech., vol. 84, part 1 pp. 13-31, 1978
16. Durst, F., and A. K. Rastogi, Theoretical and Experimental Investigations of Turbulent Flow with Separation, Turbulent Shear Flow I, pp. 208-219, New York: Springer-Verlag, 1979

Appendices

APPENDIX A

MEAN VELOCITY VECTOR

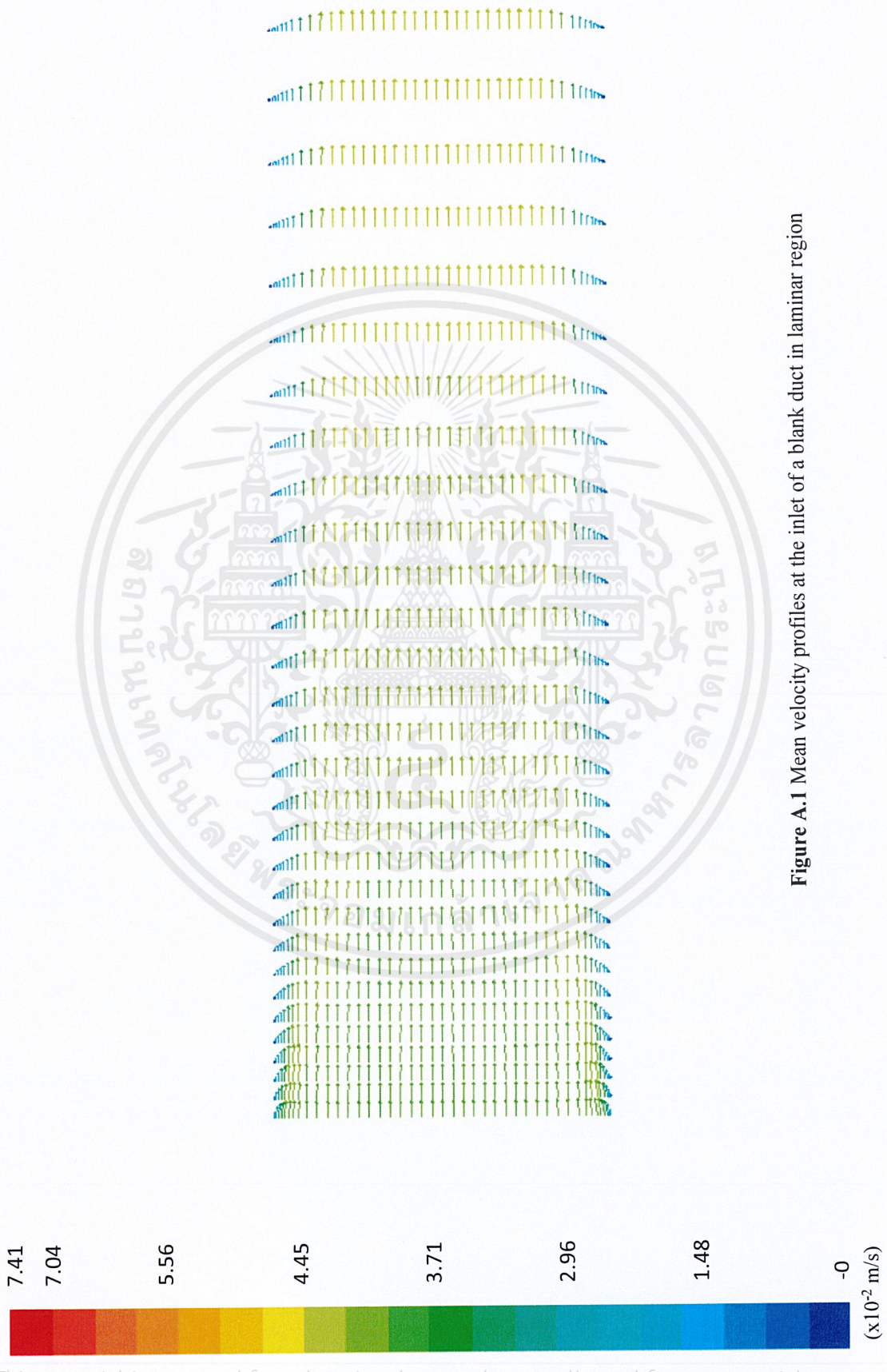

Figure A.1 Mean velocity profiles at the inlet of a blank duct in laminar region

Figure A.2 Mean velocity profiles at the inlet of a blank duct in turbulent region

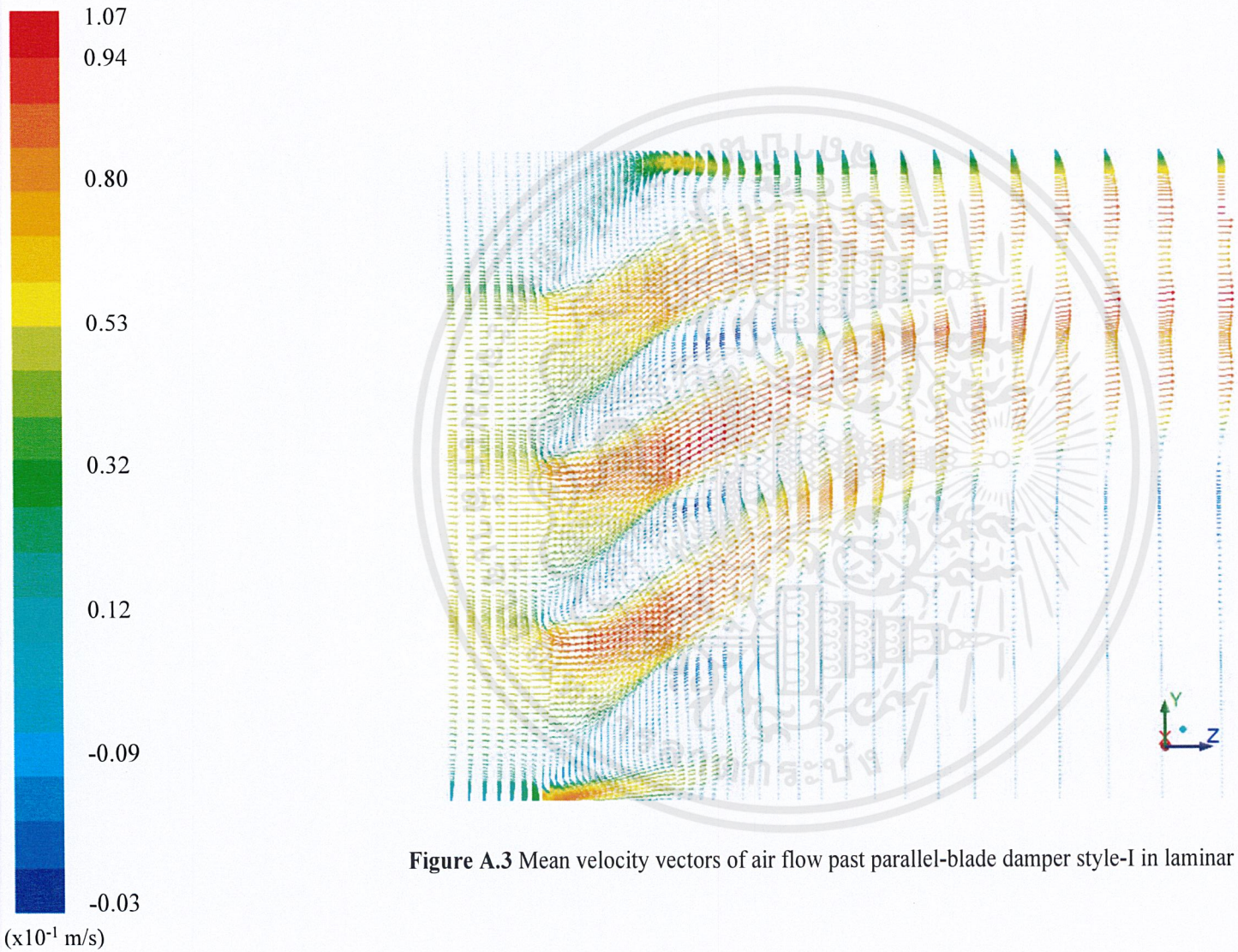

Figure A.3 Mean velocity vectors of air flow past parallel-blade damper style-I in laminar region

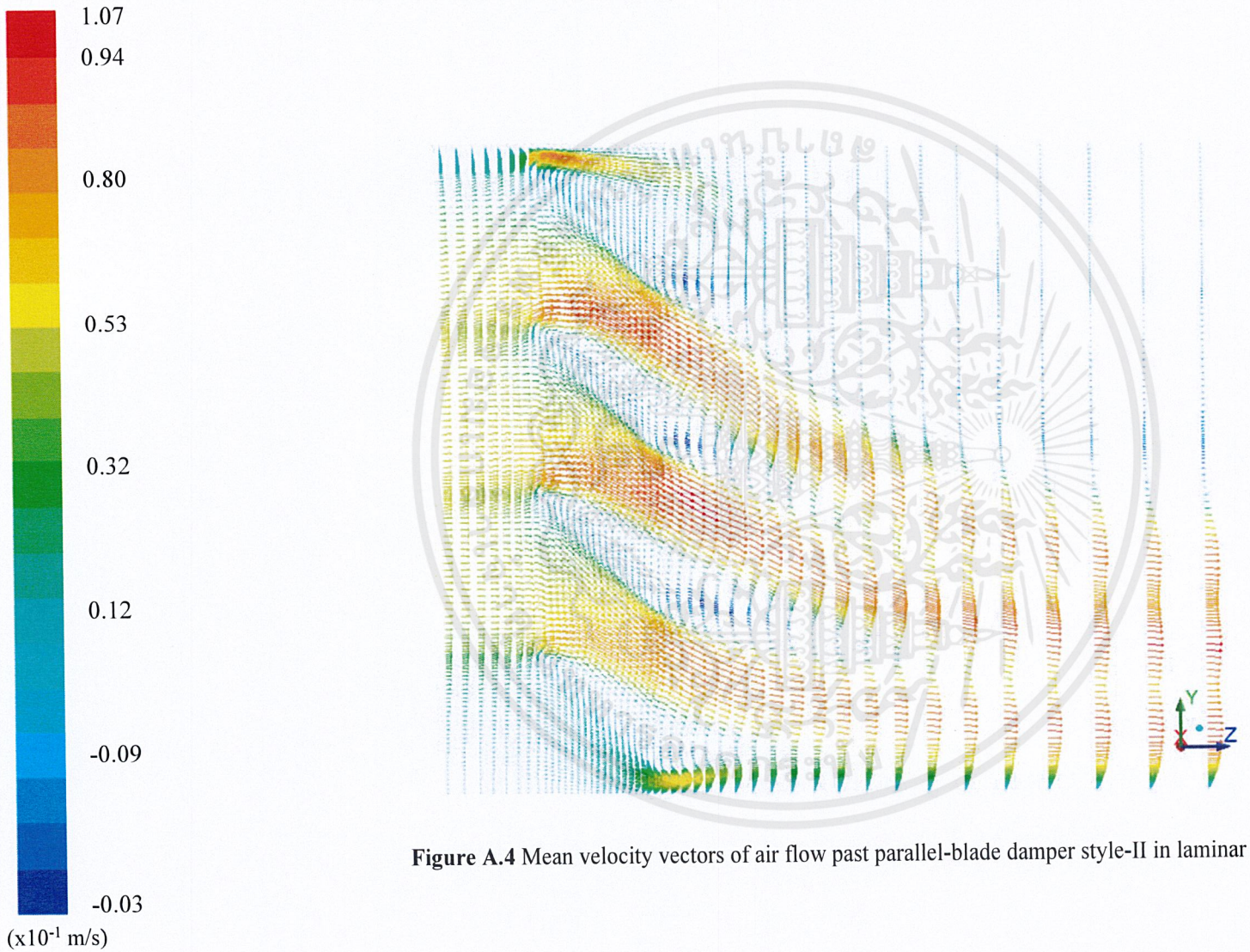

Figure A.4 Mean velocity vectors of air flow past parallel-blade damper style-II in laminar region

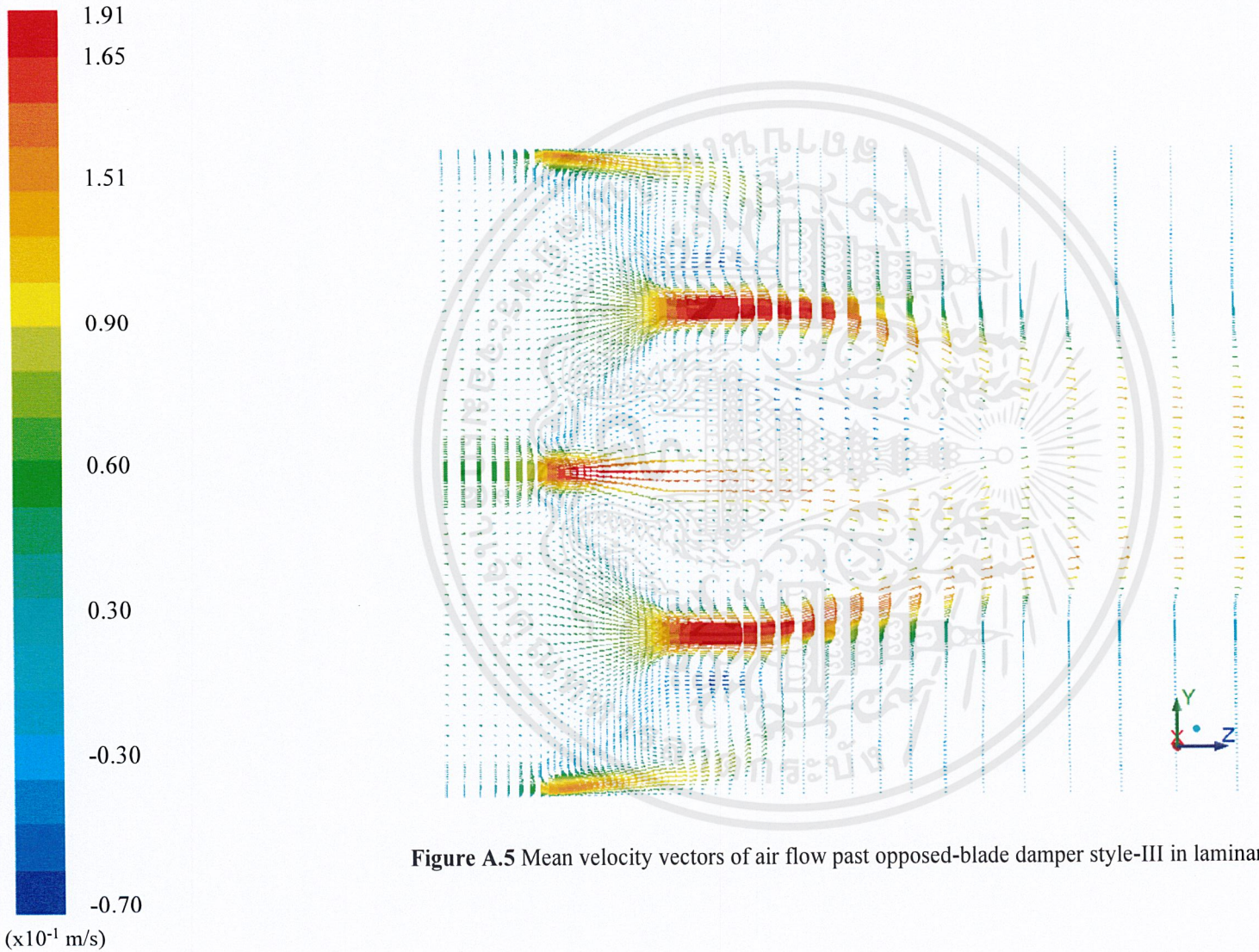

Figure A.5 Mean velocity vectors of air flow past opposed-blade damper style-III in laminar region

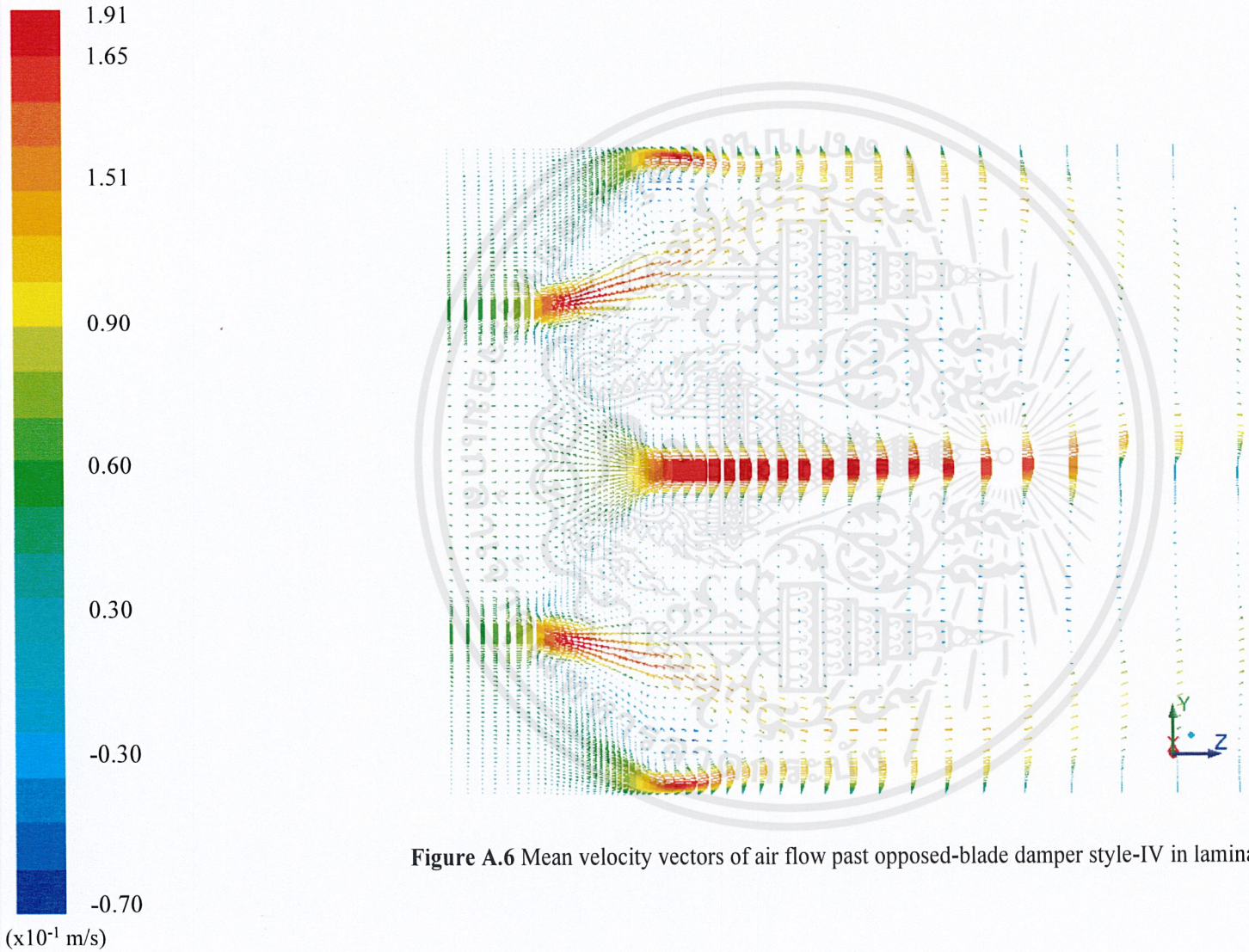

Figure A.6 Mean velocity vectors of air flow past opposed-blade damper style-IV in laminar region

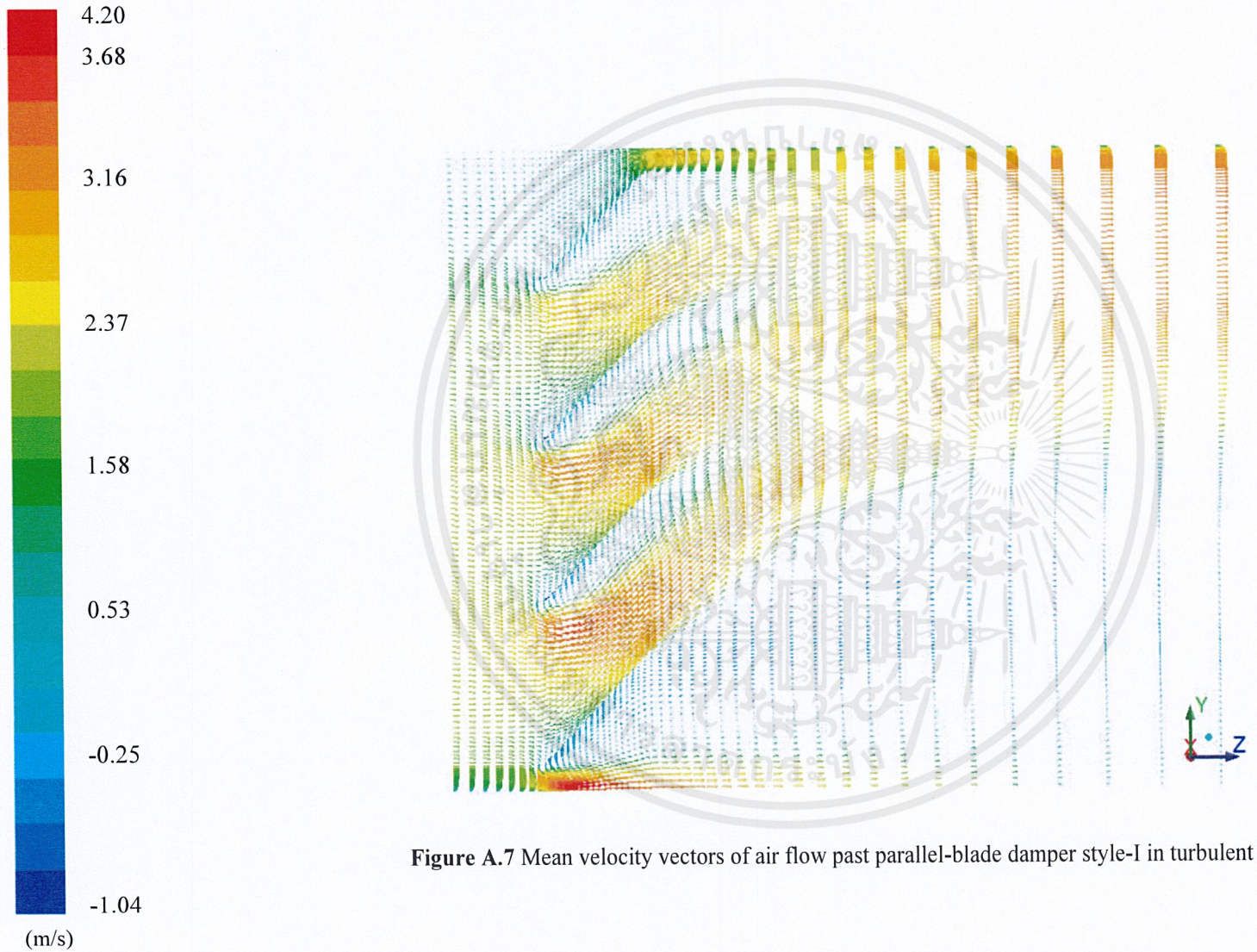

Figure A.7 Mean velocity vectors of air flow past parallel-blade damper style-I in turbulent region

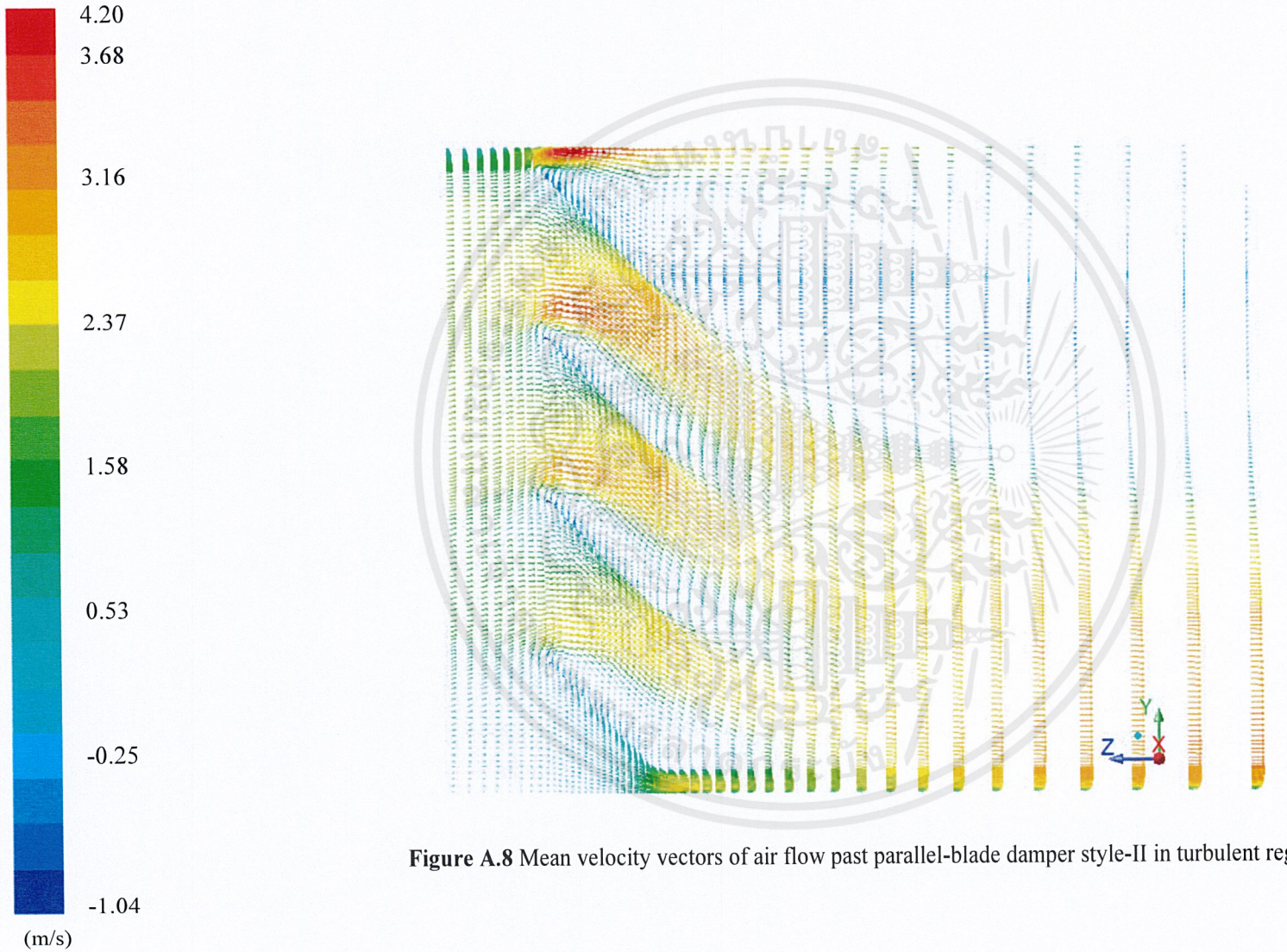

Figure A.8 Mean velocity vectors of air flow past parallel-blade damper style-II in turbulent region

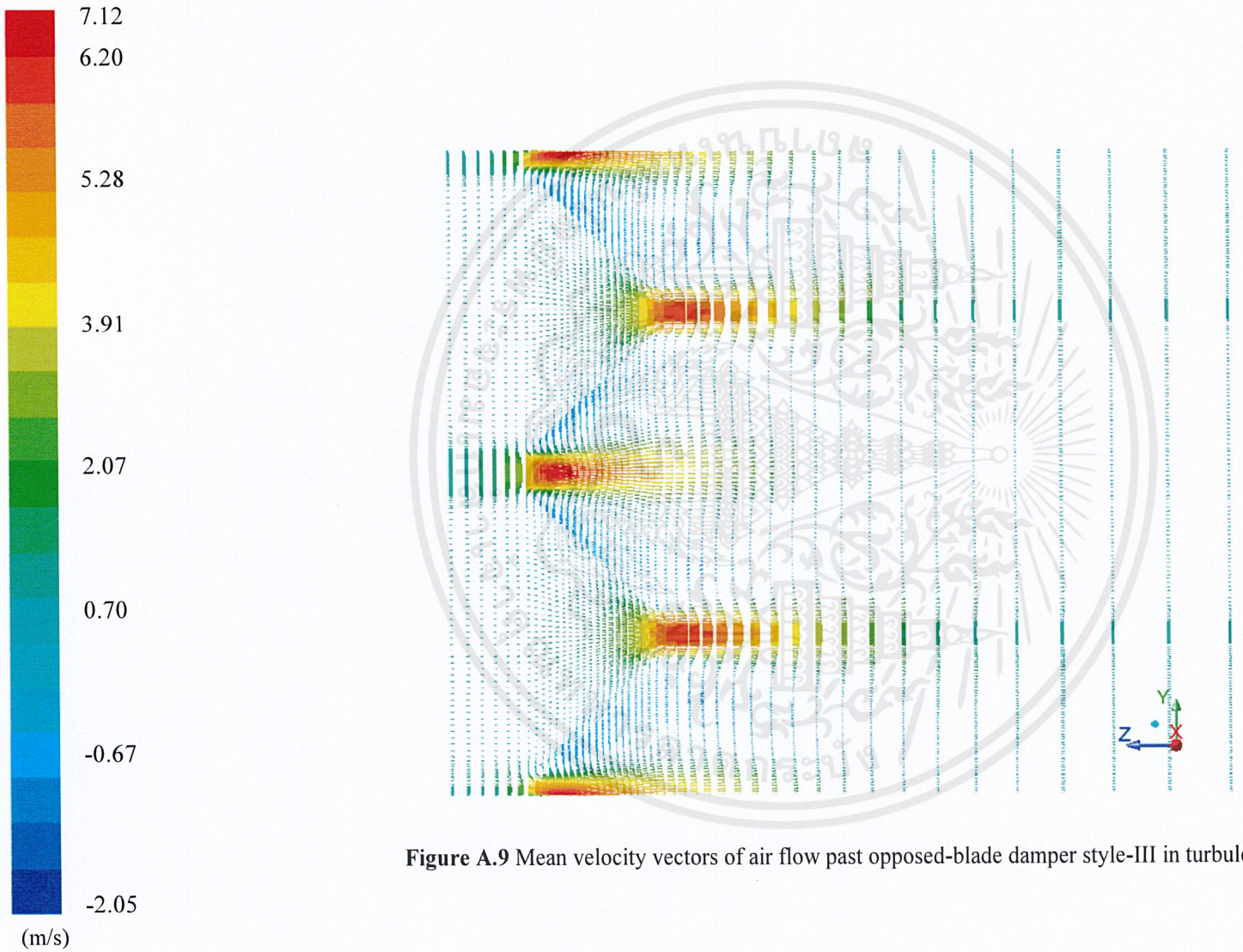

Figure A.9 Mean velocity vectors of air flow past opposed-blade damper style-III in turbulent region

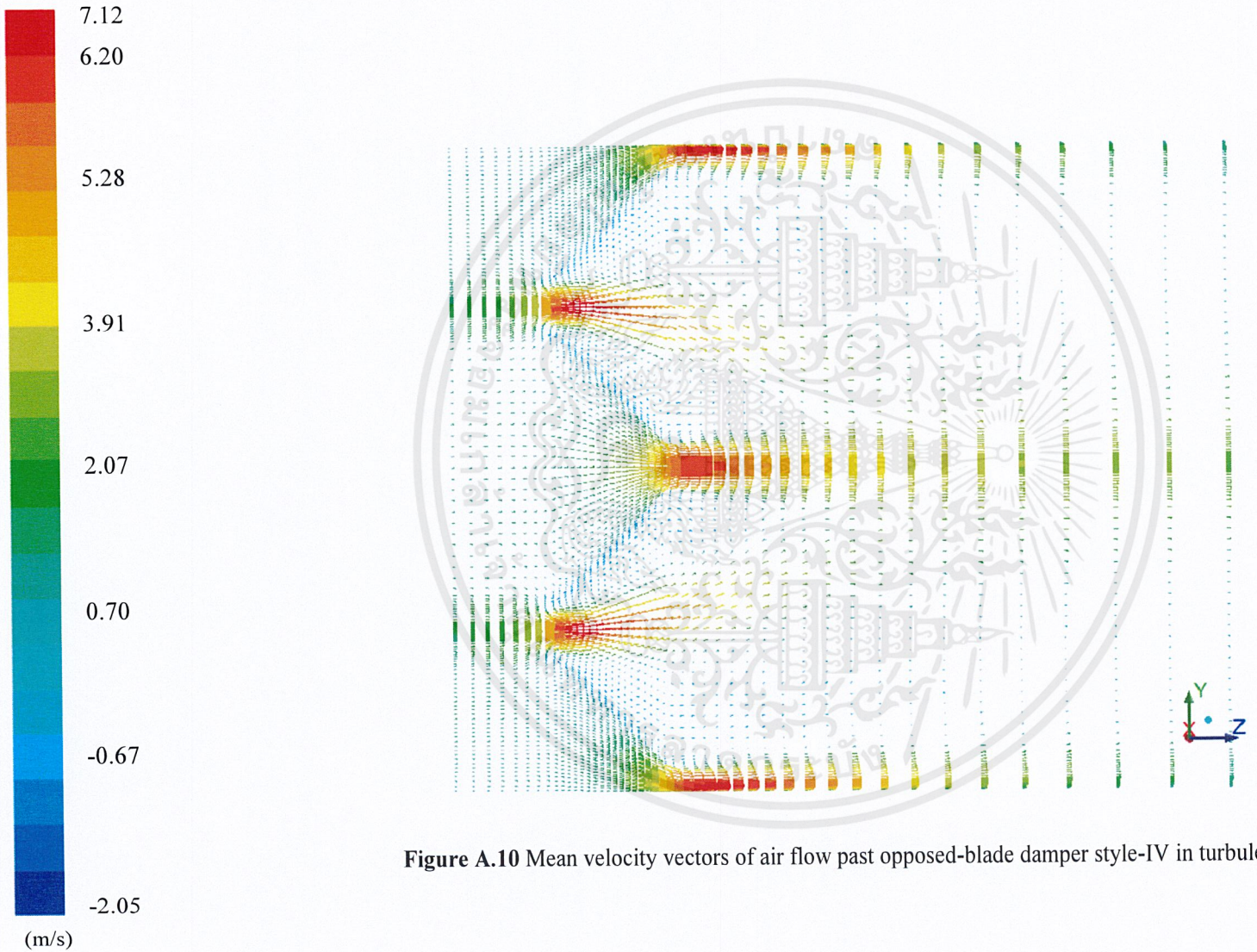

Figure A.10 Mean velocity vectors of air flow past opposed-blade damper style-IV in turbulent region

APPENDIX B

THE SEMI-IMPLICIT METHOD FOR PRESSURE LINKED EQUATIONS (SIMPLE) ALGORITHM

SIMPLE stands for Semi Implicit Method for Pressure-linked Equations. This algorithm was introduced by Patankar and Spalding (1972) [5]. This method can be demonstrated by two-dimensional laminar steady flow equations in Cartesian co-ordinates.

$$a_{i,J}u_{i,J} = \sum a_{nb}u_{nb} + \left(p_{I-1,J} - p_{I,J}\right)A_{i,J} + b_{i,J} \tag{B-1}$$

$$a_{I,j}v_{I,j} = \sum a_{nb}v_{nb} + \left(p_{I,J-1} - p_{I,J}\right)A_{I,j} + b_{I,j} \tag{B-2}$$

First, the pressure field p^* (guessed pressure) is guessed. Then, substituting p^* into equations (B-1) and (B-2) to yield u^* and v^* as follows

$$a_{i,J}u^*_{i,J} = \sum a_{nb}u^*_{nb} + \left(p^*_{I-1,J} - p^*_{I,J}\right)A_{i,J} + b_{i,J} \tag{B-3}$$

$$a_{I,j}v^*_{I,j} = \sum a_{nb}v^*_{nb} + \left(p^*_{I,J-1} - p^*_{I,J}\right)A_{I,j} + b_{I,j} \tag{B-4}$$

Then, the pressure correction and velocities correction can be defined as follows

$$p' = p - p^* \tag{B-5a}$$

$$u' = u - u^* \tag{B-5b}$$

$$v' = v - v^* \tag{B-5c}$$

Subtraction equations (B-3) and (B-4) from equations (B-1) and (B-2), respectively. Then, using correction formulae equations (B-5a) to (B-5c) to yield equations (B-6) and (B-7).

$$a_{i,J}u'_{i,J} = \sum a_{nb}u'_{nb} + \left(p'_{I-1,J} - p'_{I,J}\right)A_{i,J} \tag{B-6}$$

$$a_{I,j}v'_{I,j} = \sum a_{nb}v'_{nb} + \left(p'_{I,J-1} - p'_{I,J}\right)A_{I,j} \tag{B-7}$$

Approximating equations (B-6) and (B-7) by eliminate $\sum a_{nb}u'_{nb}$ and $\sum a_{nb}v'_{nb}$. Equations (B-6) and (B-7) become

$$u'_{i,J} = d_{i,J}\left(p'_{I-1,J} - p'_{I,J}\right) \tag{B-8}$$

$$v'_{I,j} = d_{I,j}\left(p'_{I,J-1} - p'_{I,J}\right) \tag{B-9}$$

where $d_{i,J} = \dfrac{A_{i,J}}{a_{i,J}}$ and $d_{I,j} = \dfrac{A_{I,j}}{a_{I,j}}$

Substituting equations (B-8) and (B-9) into equations (B-5b) and (B-5c), respectively. Then, rearranging the results to yield equations (B-10) and (B-11).

$$u_{i,J} = u^*_{i,J} + d_{i,J}\left(p'_{I-1,J} - p'_{I,J}\right) \tag{B-10}$$

$$v_{I,j} = v^*_{I,j} + d_{I,j}\left(p'_{I,J-1} - p'_{I,J}\right) \tag{B-11}$$

Similar expressions exist for $u_{i+1,J}$ and $v_{I,j+1}$:

$$u_{i+1,J} = u^*_{i+1,J} + d_{i+1,J}\left(p'_{I,J} - p'_{I+1,J}\right) \tag{B-12}$$

$$v_{I,j+1} = v^*_{I,j+1} + d_{I,j+1}\left(p'_{I,J} - p'_{I,J+1}\right) \tag{B-13}$$

where $d_{i+1,J} = \dfrac{A_{i+1,J}}{a_{i+1,J}}$ and $d_{I,j+1} = \dfrac{A_{I,j+1}}{a_{I,j+1}}$

The velocity field will satisfy continuity equation. The discretized continuity equation is given by

$$\left((\rho uA)_{i+1,J} - (\rho uA)_{i,J}\right) + \left((\rho vA)_{I,j+1} - (\rho vA)_{I,j}\right) = 0 \tag{B-14}$$

Substituting the corrected velocity into equation (C-14) yields the pressure correction equation.

$$a_{I,J}p'_{I,J} = a_{I+1,J}p'_{I+1,J} + a_{I-1,J}p'_{I-1,J} + a_{I,J+1}p'_{I,J+1} + a_{I,J-1}p'_{I,J-1} + b'_{I,J} \tag{B-15}$$

where $a_{I,J} = a_{I+1,J} + a_{I-1,J} + a_{I,J+1} + a_{I,J-1}$ and the coefficients are given in Table B.1.

Table B.1 Coefficients of pressure correction equation and their values

Coefficient	Value
$a_{I+1,J}$	$(\rho dA)_{i+1,J}$
$a_{I-1,J}$	$(\rho dA)_{i,J}$
$a_{I,J+1}$	$(\rho dA)_{I,j+1}$
$a_{i,J-1}$	$(\rho dA)_{I,j}$
$b'_{I,J}$	$(\rho u^* A)_{i,J} - (\rho u^* A)_{i+1,J} + (\rho v^* A)_{I,j} - (\rho v^* A)_{I,j+1}$

The source term b' is the mass imbalance which arising from the incorrect velocity field u^* and v^*. By solving equation (B-15), the correction pressure (p') can be obtained at all points. Then, the correct pressure and correct velocities can be obtained by solving equations (B-5a) and (B-10) to (B-13), respectively.

The earlier approximation does not affect the final solution because the correction pressure and correction velocities will be zero in converged solution giving $p^* = p$, $u^* = u$ and $v^* = v$.

The pressure correction is susceptible to divergence unless some under-relaxation is used during the iterative process and new, improved, pressure p^{new} are obtained with

$$p^{new} = p^* + \alpha_p p' \tag{B-16}$$

where α_p is the pressure under-relaxation factor.

A correct choice of under-relaxation factor (α) is essential for cost-effective simulations. Too large value of α may lead to divergent iterative solutions and a value which is too small will cause extremely slow convergence. Unfortunately, the values of under-relaxation factors are flow dependent and must be sought on a case-by-case basis.

The procedure of SIMPLE algorithm is shown in Figure B.1.

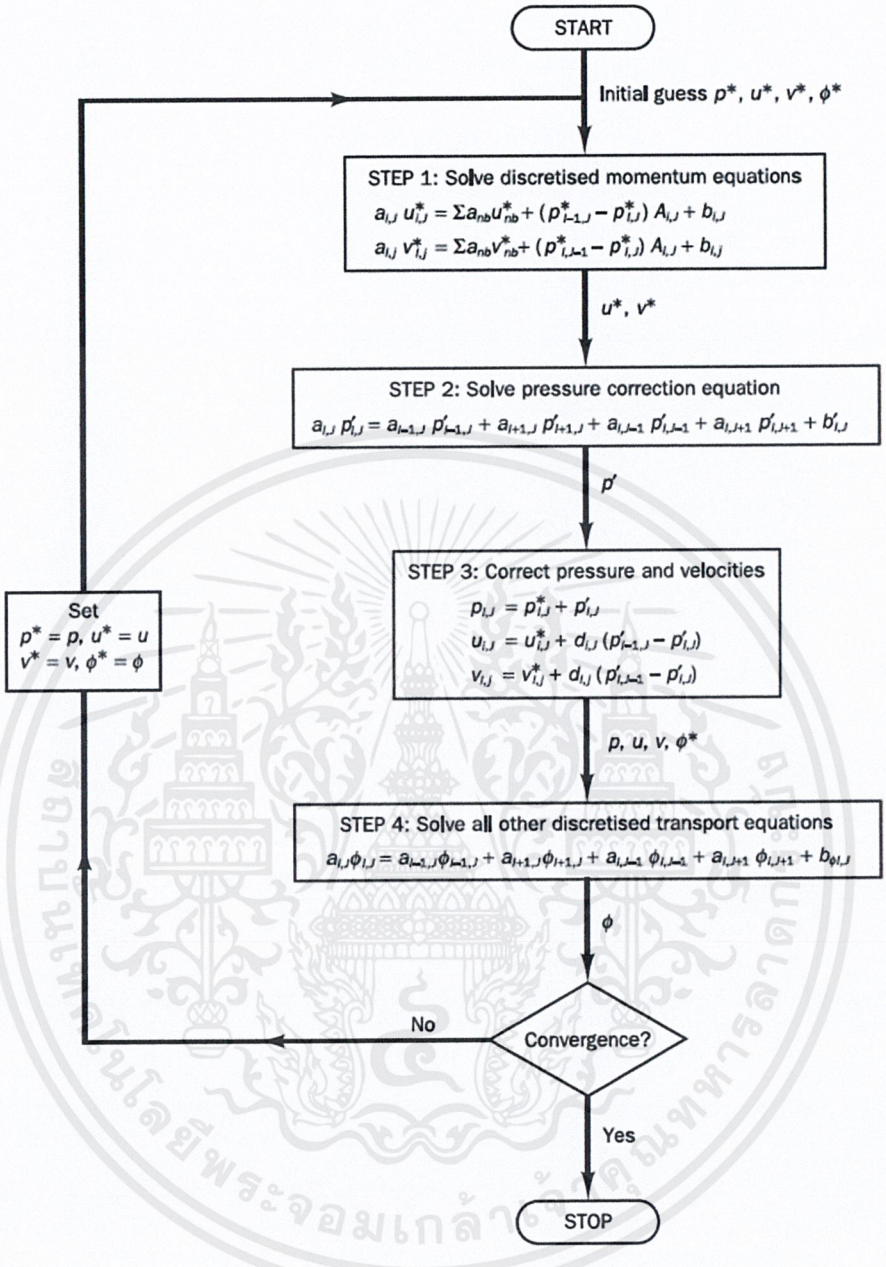

Figure B.1 The SIMPLE algorithm

APPENDIX C

APPLICATION EXAMPLES OF ANSYS FLUENT

1.Run the Fluent 14.5 ⟶ select Dimension is 3D ⟶ select Working Directory as the location to store data

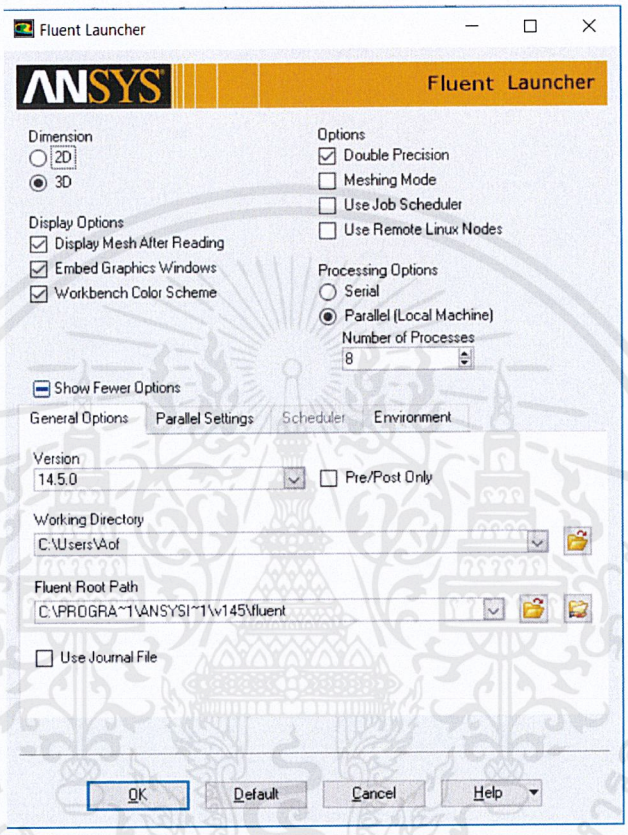

Figure C.1 The Fluent 14.5 launch

2. Run the file that imported from Gambit 2.4.6 choose File⟶Read⟶Mesh⟶choose file's type ".msh"⟶OK

3.When the grid file is run successfully, will start setting by choose General⟶Solver ⟶choose Time = Steady

4.Determine the model to simulate turbulent flow by choose Model⟶Viscous⟶Model = k-epsilon for turbulent flow case, = laminar for laminar flow case

5.Determine the used in the simulation by choose Material ⟶ Create/Edit ⟶ edit the density and viscosity

6.Define boundary conditions

- Damper: Boundary conditions ⟶ Edit ⟶ Momentum ⟶ Wall Motion = Stationary Wall ⟶ Shear condition = No Slip
- Inlet: Boundary conditions⟶Edit⟶Momentum⟶define Velocity Magnitude (m/s) = 0.0375 for laminar flow, = 1.5 for turbulent flow ⟶ define Turbulent Intensity (%) = 5, Hydraulic Diameter (m) = 0.4

- Outlet: Boundary conditions → Edit → define Turbulent Intensity (%) = 5, Hydraulic Diameter (m) = 0.4

7.Define Solution Methods → Scheme = SIMPLE, Gradient = Least Squares Cell Based, Pressure = Standard, Momentum = Second Order Upwind, Turbulent Kinetic Energy = Second Order Upwind, Turbulent Dissipation Rate = Second Order Upwind
8.Define Solution Controls in case the solution diverges by reducing the control solution → Under-Relaxation Factors → by decrease Momentum to 0.3, increase Pressure to 0.7
9.Define Solution Initialization→Solution Initialization→Initialize
10.Then start calculating by Run Calculation→define Number of Iterations→Calculate
11.Collection of simulation results after calculation. First, create a plane to store data in target area by choose Surface→ Line/Rake → define area along the duct length then collect simulation results by choose Results→Plots→XY Plot→Set Up

- Plot Direction: X=0, Y=0, Z=1
- Y Axis Function: Velocity, Z Velocity
- X Axis Function: Direction Vector
- Surfaces: choose the collecting line→Plot

To display simulation results with contours by choose Graphics and Animation →Graphics→Contours→ then select the desired variable to display
12.Save the simulation data by choose File→Write→Case&Data→ define the file name and choose file's type is ".gz", then choose collecting folder

BIOGRAPHY

Name: Satapan Phapatarinan

Date of Birth: 23 September 1994

Address: 99/454 Soi Suanluang, Bang Kho, Chom Thong, Bangkok, 10150

E-mail: satapan.p@hotmail.com

Academic Background

- 2009 – 2012: High School
  Hatyaiwittayalai School, Hat Yai, Songkhla
- 2013 – Present: Bachelor of Petrochemical Engineering
  Faculty of Engineering, King Mongkut's Institute of Technology Ladkrabang

Experiences

- June 2016 – July 2012: Northern Petroleum Development Center
  Process Engineer, Refinery Division